An essential role of high-molecular-weight kininogen in endotoxemia

Aizhen Yang,[1]* Zhanli Xie,[1]* Bo Wang,[1]* Robert W. Colman,[2] Jihong Dai,[2,3] and Yi Wu[1,2]

[1]Cyrus Tang Hematology Center, Collaborative Innovation Center of Hematology, Soochow University, Suzhou, China
[2]Sol Sherry Thrombosis Research Center, Temple University School of Medicine, Philadelphia, PA
[3]Department of Pathology and Laboratory Medicine, Rutgers–New Jersey Medical School, Newark, NJ

In this study, we show that mice lacking high-molecular-weight kininogen (HK) were resistant to lipopolysaccharide (LPS)–induced mortality and had significantly reduced circulating LPS levels. Replenishment of HK-deficient mice with human HK recovered the LPS levels and rendered the mice susceptible to LPS-induced mortality. Binding of HK to LPS occurred through the O-polysaccharide/core oligosaccharide, consistent with the ability to bind LPS from *K. pneumoniae*, *P. aeruginosa*, *S. minnesota*, and different *E. coli* strains. Binding of LPS induced plasma HK cleavage to the two-chain form (HKa, containing a heavy chain [HC] and a light chain [LC]) and bradykinin. Both HKa and the LC, but not the HC, could disaggregate LPS. The light chain bound LPS with high affinity (K_d = 1.52 × 10^{-9} M) through a binding site in domain 5 (DHG15). A monoclonal antibody against D5 significantly reduced LPS-induced mortality and circulating LPS levels in wild-type mice. Thus, HK, as a major LPS carrier in circulation, plays an essential role in endotoxemia.

INTRODUCTION

LPS is a major component of the outer membrane of gram-negative bacteria. In the initial phase of infection, LPS released from the bacteria triggers potent innate immune responses and serves as an early warning signal that primes the host immune system against further infection. However, when the LPS response is not properly controlled, endotoxemia, caused by the persistence of LPS in circulation, can cause excessive or unwanted inflammation, leading to fatal septic shock syndrome (Davies and Cohen, 2011). Clinical studies in patients with gram-negative sepsis have shown that circulating LPS level is correlated with illness severity (Acute Physiology and Chronic Health Evaluation II), the onset and amount of organ dysfunction (Sequential Organ Failure Assessment), and intensive care unit mortality (Davies and Cohen, 2011; Cohen et al., 2015; Gotts and Matthay, 2016). Over the past several decades, there have been enormous advances in our understanding of the cellular and molecular basis of the host response to LPS. Characterization of these events has led to the design of LPS removal therapies that attempt to reduce the high morbidity and mortality associated with sepsis (Ronco, 2014; Cohen et al., 2015), but to date, none of these approaches have been successful (Harm

et al., 2014; Ronco, 2014), demonstrating that the interaction of LPS with host proteins leading to endotoxemia is very complex. In particular, the host protein(s) that is exploited by LPS to persist in circulation remains an enigma (Cohen et al., 2015). Therefore, defining the mechanisms by which LPS interacts with plasma proteins is important, because this should offer new insights into the mechanism underlying endotoxemia that could then lead to strategies that promote LPS clearance and improve outcomes in patients with sepsis.

The common structural patterns in LPS molecules derived from a range of diverse bacterial species are recognized by a cascade of LPS receptors and accessory proteins. LPS molecules, because of their amphipathic nature, form large aggregates in the aqueous environment. In the earliest cell-mediated events after LPS release from bacteria, plasma LPS-binding protein (LBP) binds to the LPS molecules and catalyzes the release of LPS monomers from LPS aggregates (Lei and Morrison, 1988). This protein-glycolipid complex, with a stoichiometry of 1:1, is recognized with high specificity by CD14; LBP therefore acts to transfer LPS to CD14. CD14 is a glycosylphosphatidylinositol-anchored protein, found on the surface of monocytes and macrophages, that acts to concentrate LPS and presents monomeric LPS molecules to the MD-2–TLR4 complex (Park and Lee, 2013). Aggregation of the TLR4–MD-2 complex after LPS binding leads to the activation of multiple signaling components and the subsequent production of proinflammatory cytokines. Although the above model suggests the importance of the

---

*A. Yang, Z. Xie, and B. Wang contributed equally to this paper.

Correspondence to Yi Wu: yiwu@temple.edu

Abbreviations used: APC, allophycocyanin; BALF, bronchoalveolar lavage fluid; BK, bradykinin; CNBr, cyanogen bromide; D, domain; ES, embryonic stem; FPLC, fast protein liquid chromatography; FXII, coagulation factor XII; HC, heavy chain; HK, high-molecular-weight kininogen; HMGB, high mobility group box; KKS, kallikrein-kinin system; LAL, limulus amebocyte lysate; LBP, LPS-binding protein; LC, light chain; LK, low-molecular-weight kininogen; MPO, myeloperoxidase; pKal, prekallikrein; PS, phosphatidylserine; RU, response units; SCHK, single-chain high-molecular-weight kininogen; SPR, surface plasmon resonance.

LBP–CD14–MD-2–TLR4 pathway, studies using knockout mice have suggested that there are different requirements for each of these proteins in the response to LPS. Mice lacking CD14, MD-2, and TLR4 are resistant to a lethal dose of LPS (Haziot et al., 1996; Hoshino et al., 1999; Nagai et al., 2002), indicating that the CD14–MD-2–TLR4 pathway is essential for the LPS-induced inflammatory response in the host. In contrast, mice lacking LBP, the major LPS-binding protein in the mammalian body identified to date, have an almost normal inflammatory response to LPS in vivo (Wurfel et al., 1997). This is controversial, however, because other studies have reported an important role for LBP in vivo, through the use of deficient mice and neutralizing antibodies (Jack et al., 1997; Le Roy et al., 1999). These controversial observations suggest that LBP is not the only mediator of LPS-induced cell activation and that another LBP localized upstream of the CD14–MD-2–TLR4 pathway is critical in LPS-induced responses but remains unidentified. Although plasma proteins such as HMGB-1 (Youn et al., 2008) and cysteine-rich secretory protein LCCL domain containing 2 gene (CRISPLD2; Wang et al., 2009), as well as heparin (Heinzelmann and Bosshart, 2005), bind LPS and can transfer it to the CD14–MD-2–TLR4 complex, studies using knockout mice and inhibitors have also shown that none of these are required for LPS-induced mortality (Yanai et al., 2009; Huebener et al., 2015; Li et al., 2015; Zhang et al., 2016).

The plasma kallikrein-kinin system (KKS), also known as the intrinsic coagulation system or contact activation system, encompasses three plasma proteins, namely, coagulation factor XII (FXII), prekallikrein (pKal), and high-molecular-weight kininogen (HK; Colman and Schmaier, 1997; Wu, 2015). HK is responsible for the assembly of this system by binding to a negatively charged surface, which is the primary step for activation of this system. As a common substrate for pKal and FXII, HK is cleaved into the two-chain form HK (referred to as HKa) and bradykinin (BK). In humans, the activation of the KKS is associated with endotoxemia (Wu, 2015). Administration of LPS to normal subjects increases circulating BK levels and decreases pKal and FXII levels because of KKS activation–mediated consumption, demonstrating that LPS activates the KKS in humans (Kimball et al., 1972; DeLa Cadena et al., 1993). In patients with septic shock, pKal, FXII, and C1-inhibitor (an endogenous inhibitor of Kal and FXIIa) are also decreased, because of degradation as a result of KKS activation (Mason et al., 1970). In animal models, KKS activation is involved in LPS-induced biochemical and hemodynamic changes. In endotoxemic models in baboons, dogs, and rabbits, LPS causes the activation of FXII and pKal, leading to the cleavage of HK to HKa and the release of BK (Gallimore et al., 1978; Paloma et al., 1992; Pixley et al., 1992). Recently we reported that HK is capable of binding to phospholipids, resulting in its cleavage to HKa (Yang et al., 2014). In vitro, LPS activates pKal and FXII in human plasma, leading to HK cleavage into the two-chain form HKa (Morrison and Cochrane, 1974; Roeise et al., 1988). Our previous study showed

that HKa stimulates cytokine and chemokine production in human monocytes (Khan et al., 2006). These in vivo and in vitro observations suggest that the KKS is important in the pathogenesis of sepsis (Martínez-Brotóns et al., 1987; Colman, 1994; Colman and Schmaier, 1997; Hack and Colman, 1999). To date, numerous studies have attempted to use KKS inhibitors in the treatment of sepsis, but none of these have proved to be effective (DeLa Cadena et al., 1993; Jansen et al., 1996), indicating that the role of the KKS in the pathogenesis of endotoxemia and sepsis remains elusive.

In this study, using a group of KKS-knockout mice, we show that the mice lacking HK, but not other KKS components, are resistant to LPS-induced mortality and have a significant reduction in circulating LPS level, demonstrating that HK is "hijacked" by LPS to allow maintenance of its concentration in circulation; therefore, it is critical for the LPS-induced response. HK and its light chain (LC) bind to LPS with high affinity, disaggregate LPS, and significantly amplify LPS-induced TNF production. The LPS binding site in HK is mapped to the DHG15 amino acid sequence in domain 5 (D5) within the LC. A monoclonal antibody (mAb) recognizing D5 (C11C1) significantly reduces circulating LPS levels and LPS-induced mortality in WT mice. Because the phenotype of HK deficiency in response to LPS is consistent with those of CD14, MD-2, and TLR4 deficiencies, HK therefore constitutes a key element of the host response to LPS. Thus, this study has uncovered an essential role for HK in the LPS-induced inflammatory response by acting as a critical LPS carrier.

RESULTS
Mice with a deficiency in HK, but not other KKS components, are resistant to LPS–induced mortality
To assess the role of the KKS in endotoxemia, we generated a mouse strain with a deletion in the kininogen gene that encodes HK using a previously described method (Merkulov et al., 2008). The murine genome contains two homologous copies of the kininogen gene, *Kng1* and *Kng2*. Merkulov et al. (2008) demonstrated that the *Kng1* gene is responsible for the production of plasma kininogen and that the *Kng1*-derived mRNA yields three distinct isoforms of kininogen in plasma, namely, HK, low-molecular-weight kininogen (LK), and ΔmHK-D5; the *Kng2* mRNA is not translated in sufficient quantity to contribute to plasma kininogen level. Thus, we followed their strategy to delete the *Kng1* gene, resulting in a deficiency of plasma kininogen; the schematic diagram detailing this is shown in Fig. S1 A. A Kng1 floxed allele was created by replacing exon 2 and exon 3 with a PGK-Neo cassette in a BAC clone bMQ-175I03 vector (Fig. S1 A). This vector was introduced into EL350 cells. Recombination between the homologous sequences and the modification cassette led to replacement of the floxed exon 2 and exon 3 with the Frt-PGK-Neo-Frt sequence. Southern blot hybridization using the 3′ and 5′ probes revealed an 8.2-kb fragment and a 9.3-kb fragment after enzymatic digestion by HpaI in positive

embryonic stem (ES) cells (Fig. S1 B). A total of 20 cloned ES cells containing the disrupted Kng1 exons 2 and 3 were injected into 3.5-d sv129 mouse blastocysts, which were then implanted into 2.5-d CD1 pseudo-pregnant recipients. The chimeric offspring were tested for germline transmission by crossing with C57BL/6J mice. After removal of the Frt sites by crossing with Flp mice, the homozygous Kng1-floxed offspring were produced by intercrossing heterozygotes and determined by genotyping (Fig. S1 C). The floxed mice were then mated with CMV-Cre mice to generate conventional whole-body knockouts. Genotyping, using PCR analysis of tail DNA snips, revealed a PCR product derived from the null allele of 425 bp (Fig. S1 D), indicating successful excision of the sequence between the two loxP sites. Crosses between heterozygous Kng1$^{+/-}$ mice yielded homozygous knockout offspring (Kng1$^{-/-}$) in the expected Mendelian ratio. Kng1$^{-/-}$ mice did not display any obvious phenotypic abnormalities. As shown in Fig. S1 E, Kng1 mRNA was absent in the liver of Kng1$^{-/-}$ mice, although Kng2 mRNA remained expressed normally. Plasma from WT and Kng1$^{-/-}$ mice was immunoblotted with a polyclonal anti-HK antibody capable of recognizing heavy chain (HC; 138–166 aa of human kininogen). A total of three distinct kininogen species were found to be present in the plasma from WT mice (Fig. S1 F). This pattern is consistent with that observed by Merkulov et al. (2008), who characterized that the upper band (arrow 1, 110 kD) corresponds to HK; the intermediate band (arrow 2, 82 kD) corresponds to ΔmHK-D5, whose amino acid sequence spanning Thr400 through Asp482 is deleted; and the lowest band (arrow 3, 65 kD) corresponds to LK. In contrast, none of these bands were detected in plasma from Kng1$^{-/-}$ mice (Fig. S1 F). Moreover, the immunoblotting using anti-BK antibody also indicates that these three species of kininogen were absent in Kng1$^{-/-}$ plasma (Fig. S1 G). Although these antibodies recognize the sequences that both Kng1 and Kng2 do contain, both of them did not detect any kininogen proteins in the plasma of Kng1$^{-/-}$ mice despite the expression of Kng2 mRNA in liver. These results are consistent with the observations of Merkulov et al. (2008), who concluded that Kng1 is responsible for the production of plasma kininogen in mice. Thus, the Kng1$^{-/-}$ mice lack Kng1 mRNA expression in liver tissue and HK antigens in plasma.

To determine the role of HK in the pathogenesis of endotoxemia, WT and Kng1$^{-/-}$ mice were challenged with a lethal dose of LPS (50 mg/kg). Although 90% of the WT mice died within 50 h, all of the Kng1$^{-/-}$ mice were still alive at this time point (Fig. 1 A), demonstrating that HK is essential for LPS-induced mortality. Because LPS induces the activation of the KKS in human and animal models, we also observed the phenotype of mice deficient in other KKS components, namely, FXII, pKal, and BK receptors in the endotoxemia model. However, the survival rates of FXII$^{-/-}$, Klkb1$^{-/-}$, and B1RB2R$^{-/-}$ mice were similar to that of WT mice when challenged with 50 mg/kg of LPS (Fig. 1, B–D). The distinct phenotype of these KKS-knockout mice indicates that HK is

selectively required for LPS-induced mortality. When WT and Kng1$^{-/-}$ mice were challenged with TNF and polyinosinic :polycytidylic acid, their survival rates were not significantly different (Fig. 1, E and F), suggesting that the innate immune system in Kng1$^{-/-}$ mice remains intact and that the function of HK is unique in the host response to LPS.

HK deficiency ameliorates systemic inflammation and organ injury induced by LPS

To determine whether the role of HK in endotoxemia is associated with alternations in systemic inflammation, plasma cytokine levels were compared between WT and Kng1$^{-/-}$ mice. Circulating levels of TNF, IL-1β, IL-6, and HMGB-1 in Kng1$^{-/-}$ mice were significantly lower than in WT mice 4 h after LPS injection (Fig. 2 A), suggesting that HK potentiates the LPS-induced systemic proinflammatory response. To verify a role for HK in the regulation of inflammatory cytokine biosynthesis, we measured the expression levels of cytokine mRNAs in PBMCs. As shown in Fig. 2 B, PBMCs from Kng1$^{-/-}$ mice had decreased mRNA expression of TNF, IL-1β, and IL-6 compared with WT mice when challenged with LPS, indicating that HK up-regulates the mRNA expression of cytokines in leukocytes. Furthermore, we isolated inflammatory monocytes that were defined as CD11b^{high} and CD90-B220-CD49b-NK1.1-Ly-6G^{low} (Fig. 2 C) by flow cytometry. The isolated monocytes expressed Ly6C and CD115 and were negative for B220, CD3e, and Ly6G (Fig. 2 C). The levels of IL-1β and IL-6 mRNA expression in monocytes from Kng1$^{-/-}$ mice were significantly lower than in those from WT mice after challenge with LPS (Fig. 2 D). These observations suggest that HK is required for LPS-induced cytokine production.

Major organ injury is the main cause for LPS-induced death, so we compared histological changes in major organs between WT mice and Kng1$^{-/-}$ mice after LPS challenge. As shown in Fig. 3 A, the lungs of WT mice had an obvious infiltration of inflammatory cells into the interstitial and alveolar spaces, alveolar collapse, and an increase in alveolar septum thickness. In contrast, these changes were markedly ameliorated in the lungs of Kng1$^{-/-}$ mice (Fig. 3 A). Moreover, scanning electron microscopy showed abundant fibrin deposition in the alveolar space of WT mice challenged with LPS, but this was much reduced in Kng1$^{-/-}$ mice (Fig. 3 B). The permeability of the alveolar–capillary barrier is an index of LPS-induced acute lung injury, so accordingly, we measured the total protein concentration and total leukocyte number in bronchoalveolar lavage fluid (BALF). Compared with WT mice treated with PBS, WT mice challenged with LPS exhibited an increase in total protein concentration and total leukocyte number in BALF, but these parameters were significantly decreased in LPS-treated Kng1$^{-/-}$ mice (Fig. 3 C). Myeloperoxidase (MPO) is a hemeperoxidase enzyme that is abundantly expressed in neutrophils and monocytes/macrophages. There was an increase in the level of MPO in the lungs of WT mice challenged with LPS, consistent with the abundant infiltration
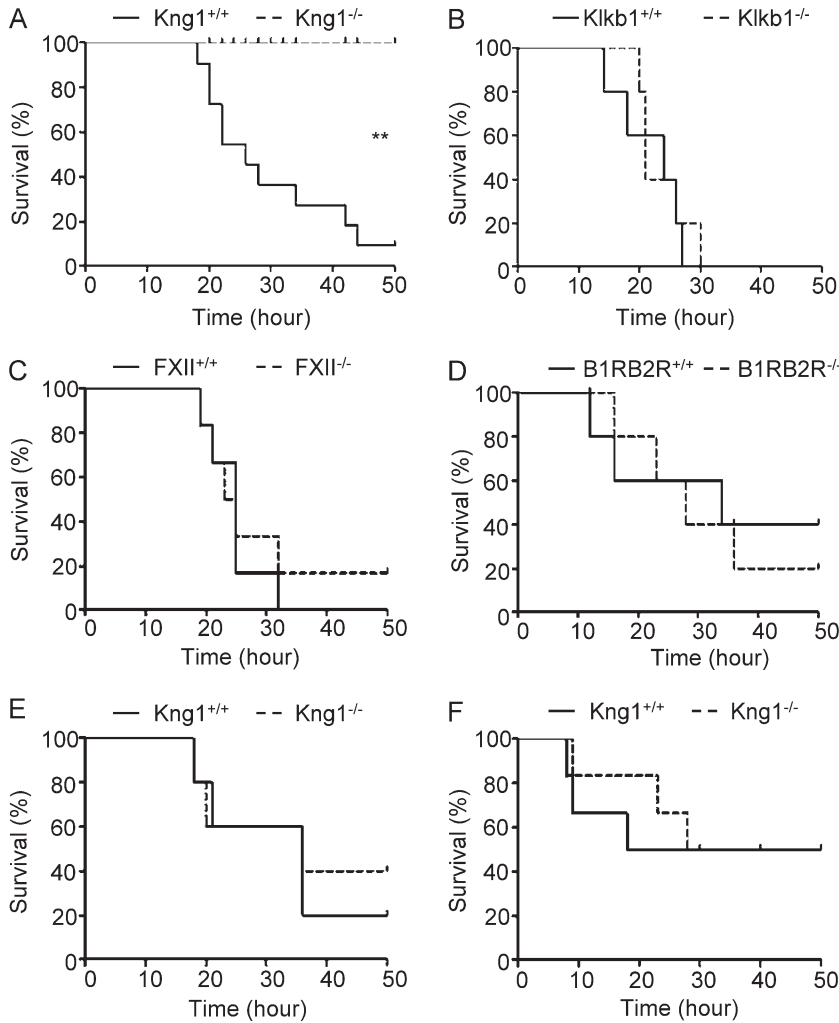
Figure 1. **HK is selectively required for LPS-induced mortality in mice.** (A–D) LPS from *E. coli* 055:B5 was injected i.p. into Kng1$^{-/-}$, Klkb1$^{-/-}$, FXII$^{-/-}$, or B1RB2R$^{-/-}$ mice and their WT littermates (control) at a dose of 50 mg/kg body weight (*n* = 15 mice/group), respectively. The survival rate was monitored and analyzed using a log-rank test. **, P < 0.01. (E and F) Kng1$^{-/-}$ mice and their WT littermates (control) were challenged by i.p. injection of 0.5 mg/kg murine TNF (E; *n* = 10), or by D-galactosamine (15 mg/mouse) pretreatment (i.p.) plus polyinosinic:polycytidylic acid (30 µg/mouse) treatment (i.v.; F; *n* = 10), and their survival rate was monitored. Statistics were analyzed using a log-rank test. Data are representative of two (B–F) or three (A) independent experiments.

of neutrophils and macrophages (Fig. 3 C). In contrast, the MPO level in the lungs of *Kng1*$^{-/-}$ mice challenged with LPS was significantly attenuated (Fig. 3 C). In addition, compared with WT mice challenged with PBS, WT mice that received LPS injections exhibited severe widespread destruction and cytoplasmic vacuolization in the liver (Fig. 3 D) and swollen tubular cells and glomerular atrophy in the kidney (Fig. 3 E). However, this damage to the liver and kidney was significantly ameliorated in *Kng1*$^{-/-}$ mice (Fig. 3, D and E). These results suggest that HK contributes to LPS-induced organ injury.

HK deficiency dramatically decreases circulating endotoxin levels in both mice and rats

To examine whether the phenotype of LPS-induced mortality in *Kng1*$^{-/-}$ mice is associated with an alteration in LPS levels, we compared circulating LPS levels between WT mice and *Kng1*$^{-/-}$ mice. At 3, 6, and 12 h after LPS injection, the circulating LPS levels in *Kng1*$^{-/-}$ mice were significantly lower than the levels in WT mice (Fig. 4 A, left). Moreover, the kinetics of circulating LPS, as indicated by the area under the curve, were reduced by ∼50% in *Kng1*$^{-/-}$ mice compared with those in

WT mice (Fig. 4 A, right). To confirm whether the reduction in LPS levels in *Kng1*$^{-/-}$ mice is directly associated with the absence of HK in plasma, human HK protein was injected into *Kng1*$^{-/-}$ mice; the reconstitution of HK in the plasma 12–36 h after injection was confirmed by Western blotting. Replenishment of HK recovered the LPS levels in plasma of *Kng1*$^{-/-}$ mice (Fig. 4 B) and significantly increased LPS-induced mortality (Fig. 4 C). There was no significant difference in LPS levels between WT mice and *TLR4*$^{-/-}$ mice when challenged with LPS (Fig. 4 D), suggesting that although *Kng1*$^{-/-}$ mice and *TLR4*$^{-/-}$ mice share the same phenotype in LPS-induced mortality, the mechanisms are different, at least with regard to the regulation of circulating LPS levels. Similar to *Kng1*$^{-/-}$ mice, HK-deficient rats also had significantly reduced levels of circulating LPS (Fig. 4 E). Collectively, these results suggest that its requirement for the maintenance of circulating LPS levels is an evolutionarily conserved function of HK.

HK is an LBP

The critical role of HK in supporting circulating LPS levels suggests that HK binds directly to LPS. To test this, human
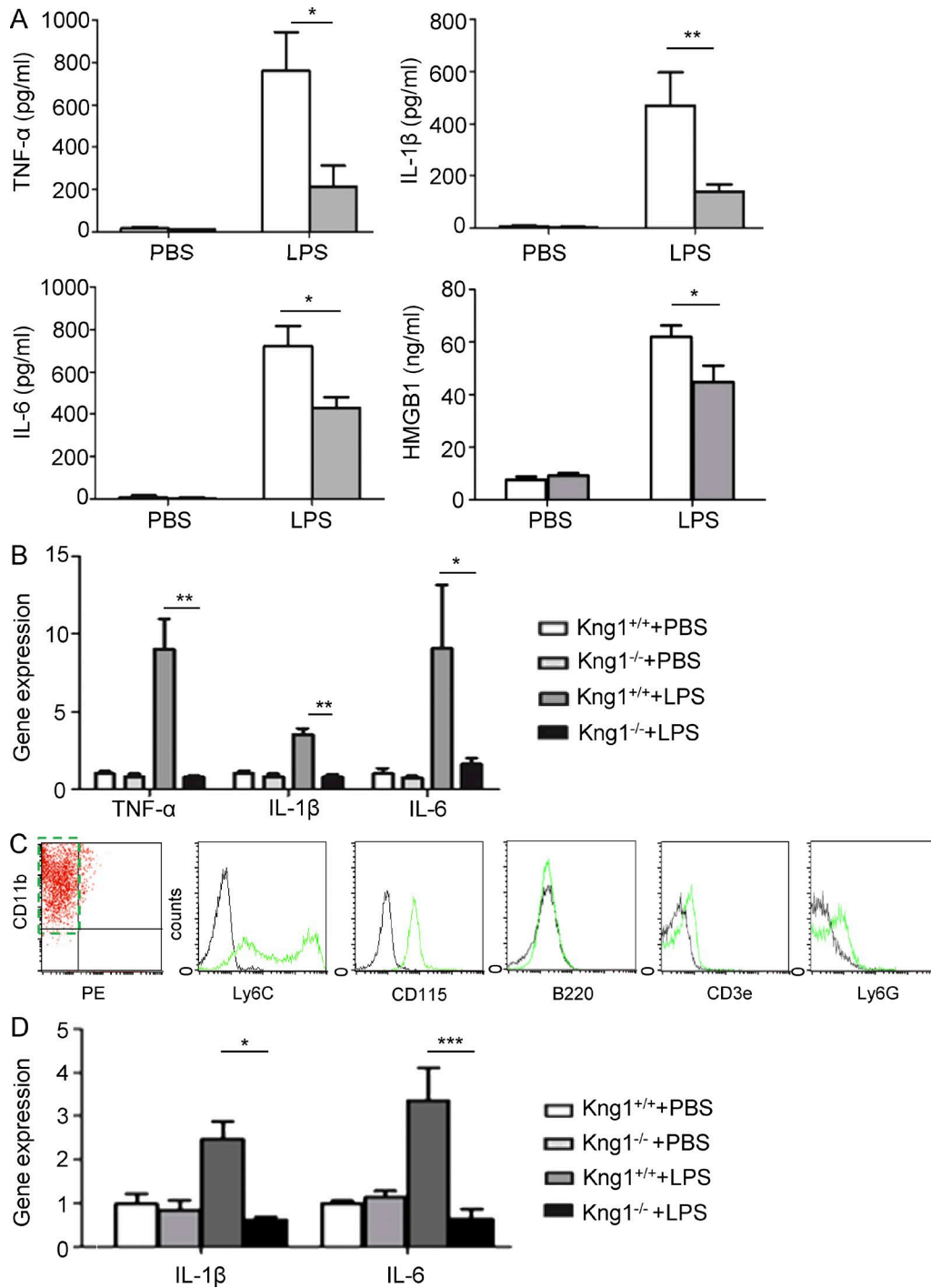
Figure 2. **HK deficiency inhibits LPS–induced cytokine production in mice.** (A and B) Kng1^{−/−} mice and their littermate control mice were challenged by PBS (control) or LPS (5 mg/kg) for 4 h, followed by collection of plasma and isolation of PBMCs. Measurements of TNF, IL-1β, IL-6, and HMGB-1 at the protein level in plasma (A) and cytokine mRNA levels in PBMCs (B) were performed as described in Materials and methods. Data were analyzed using an unpaired Student's t test and are representative of two independent experiments. *, P < 0.05; **, P < 0.01. (C) Primary murine monocytes were purified using flow cytometry with PE-labeled antibodies recognizing CD90, B220, CD49b, NK1.1, Ly-6G surface markers, and an APC-labeled anti-CD11b antibody. The purified monocytes were defined as the PE-negative and APC-positive population (dashed line rectangle). The expression of Ly6C, CD115, B220, CD3e, and Ly6G were verified by flow cytometry. (D) Kng1^{−/−} mice and their littermate control mice were challenged with PBS (control) or LPS (5 mg/kg) for 4 h, followed by isolation of monocytes. The IL-1β and IL-6 mRNA levels were measured by quantitative RT-PCR. Data were analyzed using an unpaired Student's t test and are representative of three independent experiments. *, P < 0.05; ***, P < 0.001. Data are expressed as mean ± SEM.
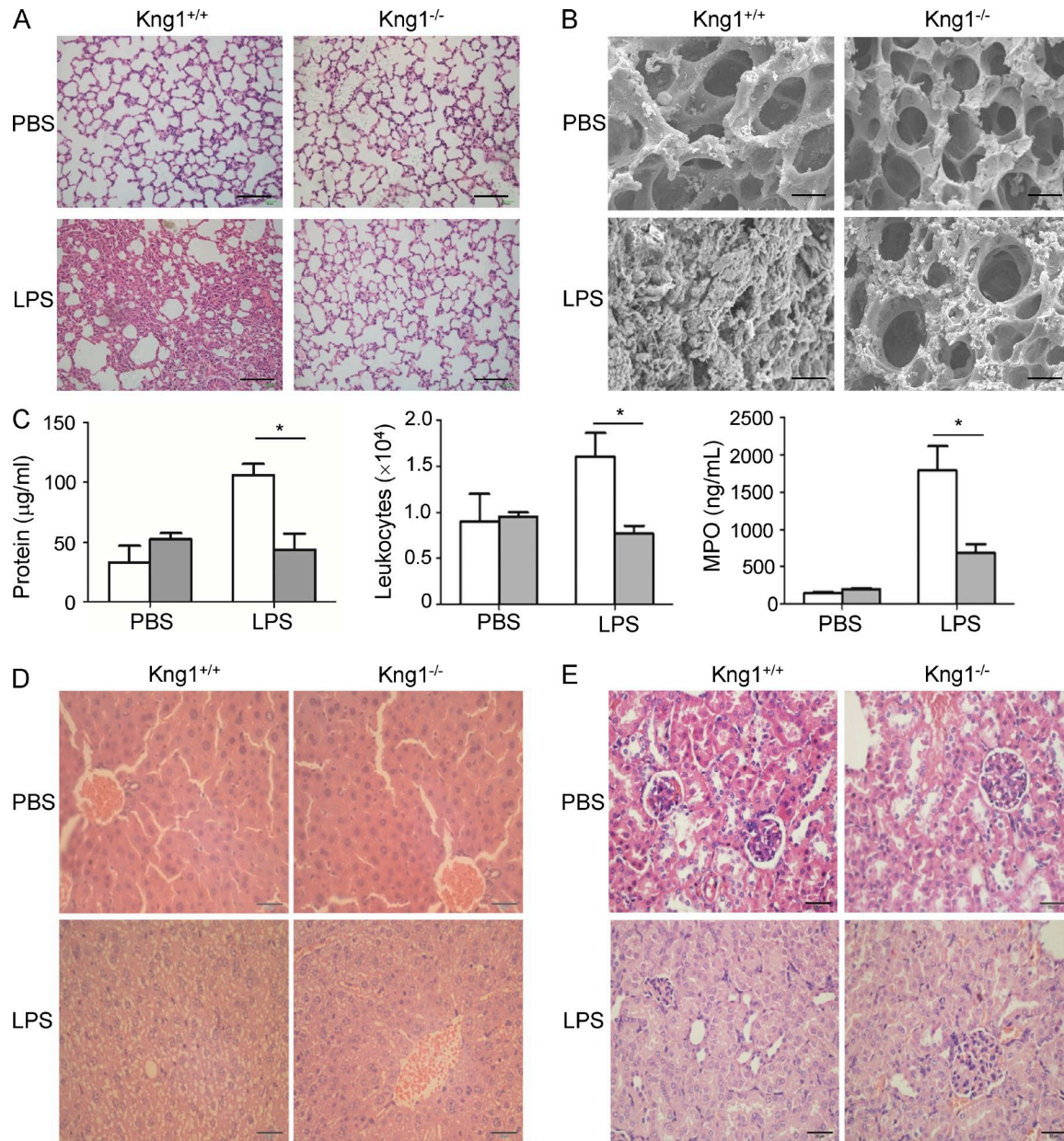
Figure 3. **HK deficiency ameliorates LPS–induced multiple organ injury.** (A and B) $Kng1^{-/-}$ mice and their littermate control mice were challenged with PBS (control) or LPS (5 mg/kg) for 48 h ($n = 6$), followed by organ harvest. Lung tissue was processed for hematoxylin and eosin (H&E) staining (A) and scanning electron microscopy (B), and the representative images are shown. Bars, 100 μm (A) and 500 μm (B). (C) Total protein concentration and white blood cells in BALF and MPO activity in lung homogenates were measured. White column, control WT mice; gray column, $Kng1^{-/-}$ mice. Data were analyzed using an unpaired Student's t test and are representative of two independent experiments. *, $P < 0.05$. Data are expressed as mean ± SEM. (D and E) Liver and kidney were processed for H&E staining, and representative images for liver (D) and kidney (E) are shown. Bars, 100 μm.

plasma was incubated with LPS-conjugated Sepharose beads, followed by detection using an anti-HK antibody. HK was found to be specifically bound to the LPS beads but not to the control beads (Fig. 5 A). To examine whether HK physically binds to LPS, HK was immobilized on microtiter plates, followed by incubation with FITC-labeled LPS. Coating of microplates with HK significantly increased FITC-LPS bind-

ing (Fig. 5 B), suggesting that HK binds directly to LPS. We have previously shown that HK binding to a cell surface or a phospholipid is dependent on the presence of $ZnCl_2$ (Zn^{2+}; Colman and Schmaier, 1997; Pixley et al., 2003). We thus tested whether zinc is involved in the binding of HK to LPS. There was no remarkable difference in the association of HK with FITC-LPS in the presence or absence of Zn^{2+} (Fig. 5 B),
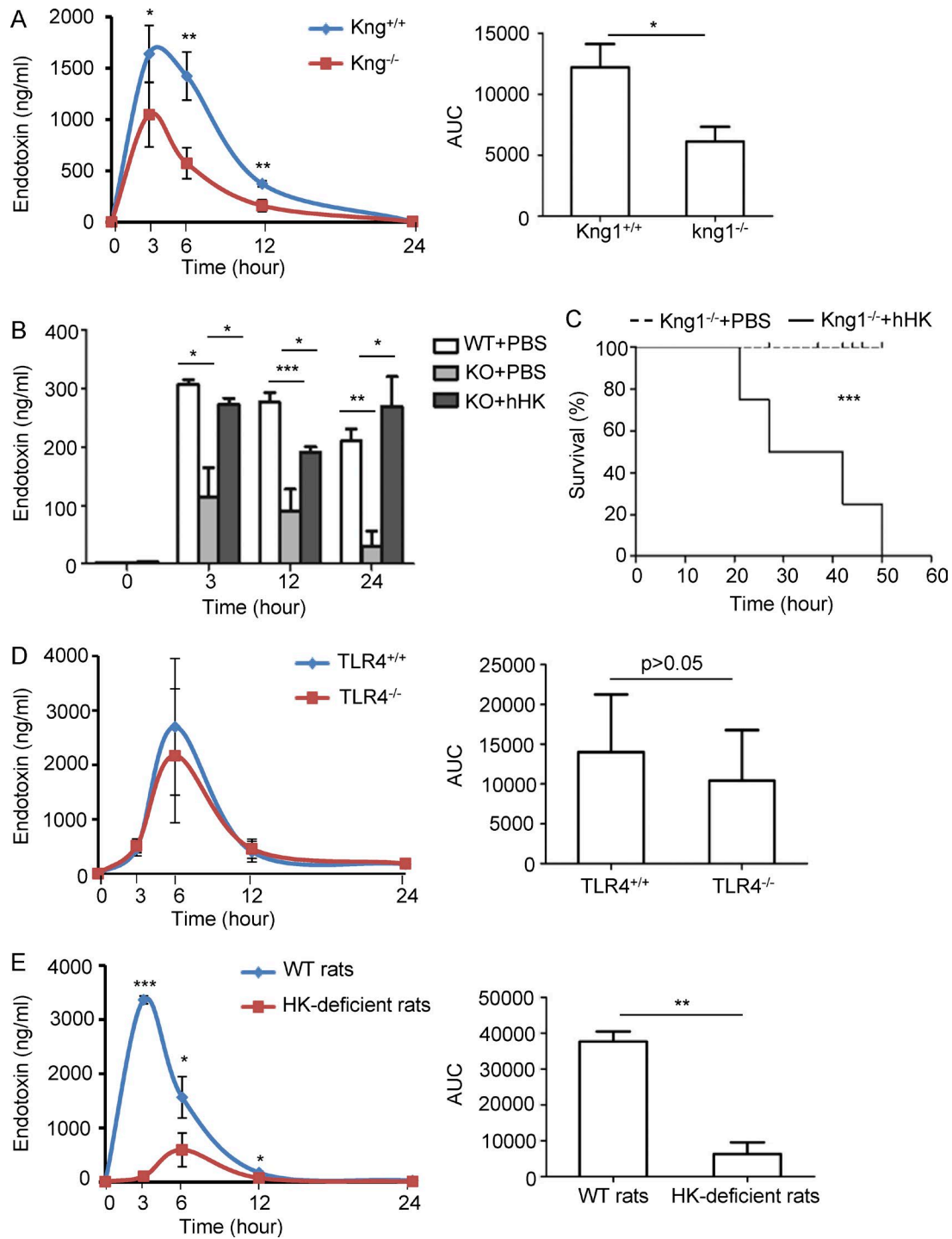
Figure 4. **HK deficiency significantly reduces circulating endotoxin levels.** (A) Kng1^{−/−} mice and their littermate control mice were challenged with LPS (5 mg/kg, i.p.), and blood was collected at the indicated time points. The LPS content in plasma was evaluated using the LAL assay (left). The area under the curve (AUC) was calculated from kinetic curves measured over 24 h (right). Data were analyzed using an unpaired Student's *t* test and are representative of five independent experiments. *, P < 0.05; **, P < 0.01. (B) After two groups of Kng1^{−/−} mice were injected with either 250 µg human HK protein or PBS, and one group of control WT mice were injected with PBS through tail vein (*n* = 8), they were challenged with 5 mg/kg LPS (i.p.). Blood was collected at the indicated time points, and plasma LPS content was evaluated using the LAL assay. Statistics were analyzed by ANOVA. *, P < 0.05; **, P < 0.01; ***, P < 0.001. Data are representative of two independent experiments. (C) After two groups of Kng1^{−/−} mice were injected with either 250 µg human HK protein or PBS (*n* = 8), they were challenged with 50 mg/kg LPS, and their survival rate was monitored. Statistics were analyzed using a log-rank test. Data are representative of two independent experiments. ***, P < 0.001. (D) Two groups of TLR4^{−/−} mice were challenged with 5 mg/kg LPS (i.p.; *n* = 8), and blood was

suggesting that zinc is not required for HK binding to LPS. To quantitate the binding affinity of HK for LPS, we performed a surface plasmon resonance (SPR) assay using a BIAcore 3000 biosensor. The sensorgrams show that HK bound to LPS with a high affinity (K_d = 1.71 × 10^{-7} M; Fig. 5 C). To understand the HK–LPS interaction in more detail, the complex formed between HK and LPS was characterized. HK–LPS complexes were isolated by size exclusion fast protein liquid chromatography (FPLC), and the HK and LPS content, as well as the stoichiometry, was subsequently determined. As shown in Fig. 5 D, free LPS eluted at 8 ml. The HK peak in the absence of LPS eluted at 20 ml, whereas HK eluted at 18 ml in the presence of LPS. These results indicate that HK shifted from an unbound state toward a LPS-bound state in the presence of LPS. The HK–LPS complex purified by FPLC was then analyzed for HK and LPS content using protein and limulus amebocyte lysate (LAL) assays, respectively. This analysis provided a molar ratio of LPS to HK of 1:1.76 ± 0.45, suggesting that on average, one LPS molecule binds one or two HK molecules in the complex. Because the FPLC patterns of the HK–LPS complex were similar in the presence and absence of 50 µM ZnCl$_2$ (Fig. S2 A), complex formation between HK and LPS in aqueous solution is not dependent on the presence of zinc.

The two–chain form of HK (cleaved HK, HKa) and its LC directly mediate LPS disaggregation

To further understand the interaction between HK and LPS, we investigated the dynamic binding of HK and its derivatives to LPS using a BODIPY FL–LPS fluorescence assay. Our recent study showed that the two-chain form of HK (cleaved HK, HKa) preferentially binds to phospholipids compared with the single-chain form of HK (Yang et al., 2014). Here we found that incubation of BODIPY FL–LPS with HKa, but not HK, markedly increased fluorescence levels (Fig. 6 A). Unlike CD14 and LBP, neither of which can disaggregate LPS, HKa alone exhibited a strong capacity in disaggregating LPS (Fig. 6 B), suggesting that HKa directly binds to aggregated LPS and releases the LPS monomer. To test the dose dependency of HKa for LPS disaggregation, we measured the effect of HKa at a variety of concentrations on the disaggregation of 30–3,000 ng/ml of BODIPY FL–LPS. As shown in Fig. 6, C–H, HKa at 0.5 µg/ml was capable of inducing LPS disaggregation, and reached a maximal effect at 600 s, whereas 2.5 µg/ml HKa exhibited disaggregation activity earlier than 0.5 µg/ml HKa. HKa at 0.5 µg/ml induced disaggregation of 3,000 ng/LPS by >40% and that of 30–1,000 ng/ml LPS by >60% (Fig. 6, C–H). These data indicate that the effect of

HKa is dose dependent. Similar to the complex formation of HK–LPS assessed using FPLC, HKa-mediated LPS disaggregation was comparable in the presence and absence of 50 µM ZnCl$_2$ (Fig. S2 B), providing additional evidence that the interaction between HK and LPS is not zinc dependent. HKa consists of two chains, a HC and a LC, which are linked by a disulfide bond after cleavage of HK. The activity of HKa in LPS disaggregation stimulated us to examine the role of HC and LC in this process. As shown in Fig. 6 A, LC, but not HC, disaggregated LPS, suggesting that LC binds to LPS.

HK binds to different LPS species through the carbohydrate region

LPS is composed of a conserved TLR4-activating moiety called lipid A and a carbohydrate region including a core oligosaccharide and a hyperdivergent O-specific polysaccharide chain. To define which region of LPS binds to HK, microtiter plate wells were coated with lipid A, delipidized LPS, or LPS at 2 µg/well, followed by incubation with 100 nM FITC-HK for 1 h. As shown in Fig. 7 A, HK bound to both LPS and delipidized LPS, but not lipid A, suggesting that HK binds LPS via the O–polysaccharide chain and/or the core oligosaccharide. Furthermore, we examined the binding of HK to different types of LPS derived from different bacterial strains. Human HK was incubated with LPS from different sources, including LPS from *E. coli* including 055:B5 (B5), 0111:B4 (B4), and 026:B6 (B6), as well as LPS from *K. pneumoniae*, *P. aeruginosa*, and *S. minnesota*, followed by incubation with polymyxin B beads to pull down the LPS. Immunoblotting with an anti-HK antibody indicates that HK associated with all these LPS species (Fig. 7 B), which is consistent with the finding of LPS binding occurring via the O–polysaccharide chain and/or the core oligosaccharide (Fig. 7 A). The SPR analysis further showed that HKa bound the LPSs from *E. coli*, *K. pneumoniae*, *P. aeruginosa*, and *S. minnesota*, albeit with different binding affinities, with K_d values ranging from 4.838 × 10^{-11} to 3.488 × 10^{-10} M (Fig. 7 C). Despite these differences, HKa potentiated TNF production in monocytes challenged with these LPS species to a similar extent (Fig. 7 D). Additionally, HKa exhibited a similar capacity to disaggregate *E. coli* 055:B5 LPS and *S. minnesota* LPS (Fig. S3). These data suggest that HK is a general pattern recognition molecule for LPS.

DHG15 amino acid region in D5 is the binding site of HK for LPS

The effect of HKa and LC on the disaggregation of LPS (Fig. 6 A) suggests that HKa interacts with LPS via its LC.

Figure 5. **HK binds to LPS with a high affinity and forms a complex in aqueous solution.** (A) Forty microliters of LPS-conjugated Sepharose beads or control-Sepharose beads were incubated with 200 μl diluted human plasma (HP; 1:1 with 1× PBS) at RT for 2 h. The beads were washed three times with PBS containing 0.1% Triton X-100, and the associated proteins were subjected to immunoblotting with an anti-HK antibody. Data are representative of five independent experiments. (B) Ninety-six-well plates were coated with 10 μg/ml of HK or BSA and were then blocked with 2% BSA. After incubation with 100 μg/ml FITC-LPS in the presence or absence of 50 μM ZnCl$_2$ at 37°C, the wells were washed, and fluorescence was measured. Statistical analysis was done using an ANOVA. ***, P < 0.001. Data are representative of two independent experiments and expressed as

To verify this possibility, we measured the binding affinity between LC and LPS using the SPR assay and found that LC bound to LPS with a high affinity (K_d = 1.52 × 10^{-9} M; Fig. 8 A). Moreover, LC enhanced LPS–stimulated TNF production in RAW264.7 cells, with its effect being lower than that of LBP (Fig. S4 A), indicating that the binding of LC does not neutralize but instead amplifies the activity of LPS.

To determine the effect of LPS on the cleavage of HK to HKa in vivo, we measured the circulating levels of BK in WT mice challenged with LPS and found that circulating BK levels were significantly increased in endotoxemic mice (Fig. S4 B). Consistent with the release of BK, when plasma from WT and *Kng1*$^{-/-}$ mice was incubated with LPS, LC was released and became bound to LPS (Fig. 8 B). Together, these data indicate that HK binds to LPS via its LC. To narrow down the binding site for LPS in the LC, recombinant D4 (376I–401T), D5 (402V–520K), and D6 (521T–644S) domain proteins were synthesized using the Bac-to-Bac baculovirus expression system. The proteins were purified from Sf9 cells and were verified by anti-His immunoblotting (Fig. 8 C). To assess the binding of these domains to LPS, they were incubated with LPS followed by pull-down with polymyxin-B beads. As shown in Fig. 8 D, only D5 was detected with polymyxin B beads in the presence of LPS, indicating that D5 physically binds to LPS. To map the binding site for LPS in D5 more precisely, eight 30-mer peptides with 15 aa overlap within D5 and the N-terminus of D6 were synthesized (Fig. 8 E, P1–P8). After preincubation with the P1–P8 peptides, 25 μg/ml LPS was incubated with 10 μg/ml LC, followed by pull-down with polymyxin B-beads. As indicated by anti-His immunoblotting and quantitation of the LC bands by densitometric analysis, peptide 6 and peptide 7 blocked the binding of LC to LPS (Fig. 8, F and G). The overlapping sequence between peptide 6 and peptide 7 was 15 aa in length, namely, DHGHKHKHGHGHGKH (referred to here as DHG15). The DHG15 region of human HK shares a high homology with the corresponding mouse HK sequence GHGHGHGHGHGHGKH. We thus tested whether this DHG15 peptide could inhibit HK binding to LPS in mouse plasma and found that it completely blocked the association of HK to LPS (Fig. 8 H), suggesting that this 15-aa sequence is an evolutionarily conserved element for binding of LPS that is shared by humans and mice.

To further determine whether the LPS–binding region DHG15 of HK is important for supporting endotox-

mean ± SEM. (C) Analysis of HK binding to LPS by SPR analysis revealing a binding affinity of K_d = 1.71 × 10^{-7} M. A representative experiment out of three independent experiments is shown. (D) FPLC profile of the HK and LPS complex. LPS (250 μg/ml) was incubated with 50 μg/ml HK at 37°C for 60 min. Samples were then loaded to the column. Samples between the two arrows were collected and subjected to measurement of protein and LPS concentrations. Solid line, HK only; dotted line, LPS only; dashed line: HK in the presence of LPS. Data are representative of three independent experiments.
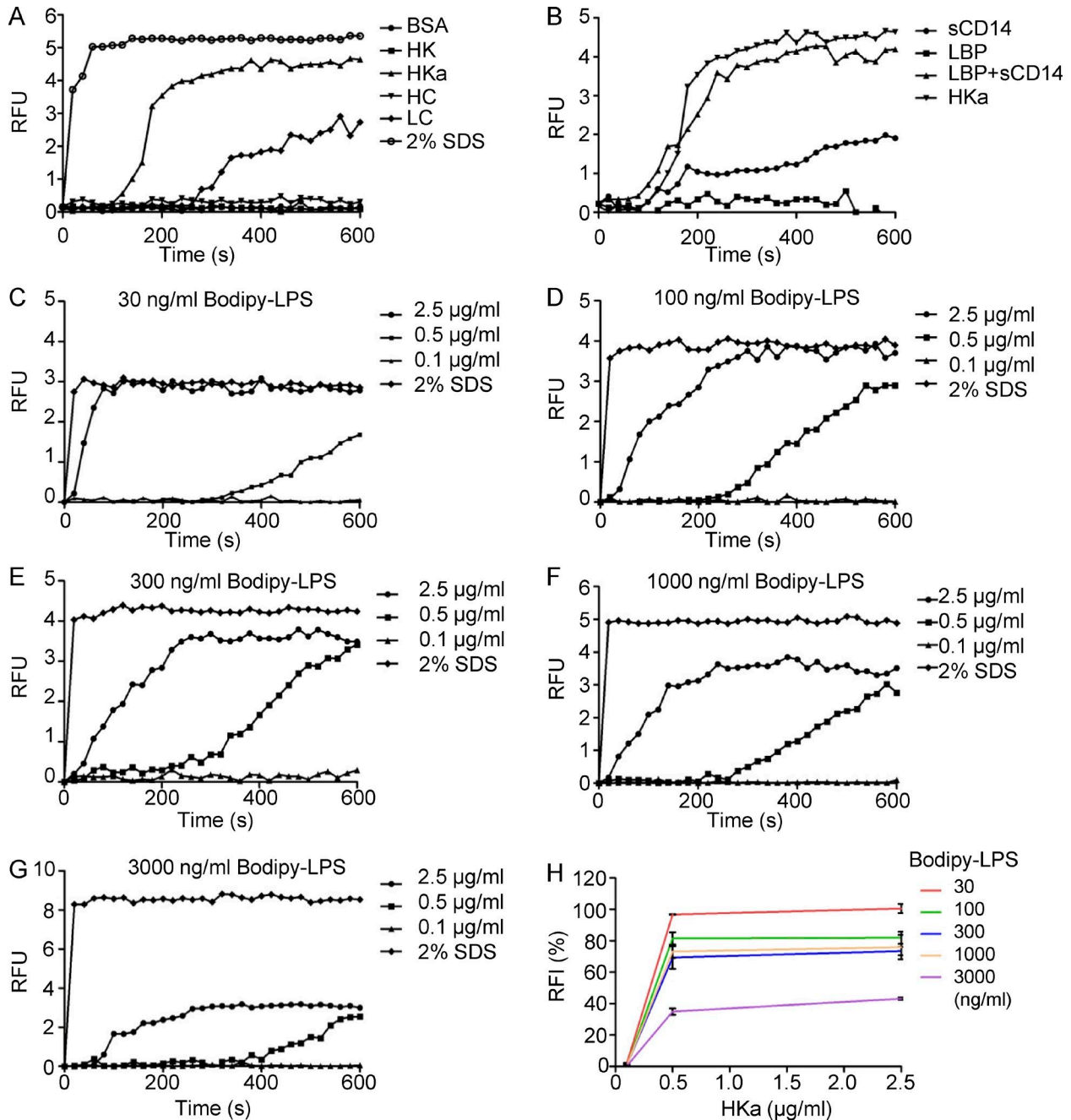
Figure 6.   **Two-chain HK (HKa) and its LC can disaggregate LPS.** (A) BODIPY FL–LPS at 50 ng/ml was suspended in 100 μl PBS. After the addition of BSA, HK, HKa, HC, or LC at 1 μg/ml, the real-time change in BODIPY FL–LPS fluorescence upon transition from the aggregated LPS state was recorded in 20-s intervals. SDS (2%) was used as the positive control. (B) BODIPY FL–LPS at 50 ng/ml was suspended in 100 μl PBS. After the addition of LBP, CD14, and LBP+CD14, or HKa at 1 μg/ml to each, the real-time change in BODIPY FL–LPS fluorescence was recorded in 20-s intervals. (C–G) BODIPY FL–LPS was suspended in 100 μl PBS at the indicated concentrations shown on the top of the graph. After 0.1, 0.5, or 2.5 μg/ml HKa was added, the real-time change in BODIPY FL–LPS fluorescence upon transition from the aggregated LPS state was recorded in 20-s intervals. The gain in fluorescence upon the addition of 2% SDS was used to define the full disaggregated state of BODIPY FL–LPS at 600 s (100% disaggregated); on this basis, the relative fluorescence intensity (RFI; %) of each curve was calculated, and the data are shown in H. Data are representative of three independent experiments and expressed as mean ± SEM.

emia, a recombinant mutant HK lacking the DHG15 (HK/ Δ492-506) was generated. The cloning strategy used for its generation is shown in Fig. S5 A. Coomassie brilliant

blue staining and immunoblotting using anti-His antibody show the size and purity of HK/Δ492-506 (Fig. S5 B). Furthermore, immunoblotting with an anti-DHG15 antibody
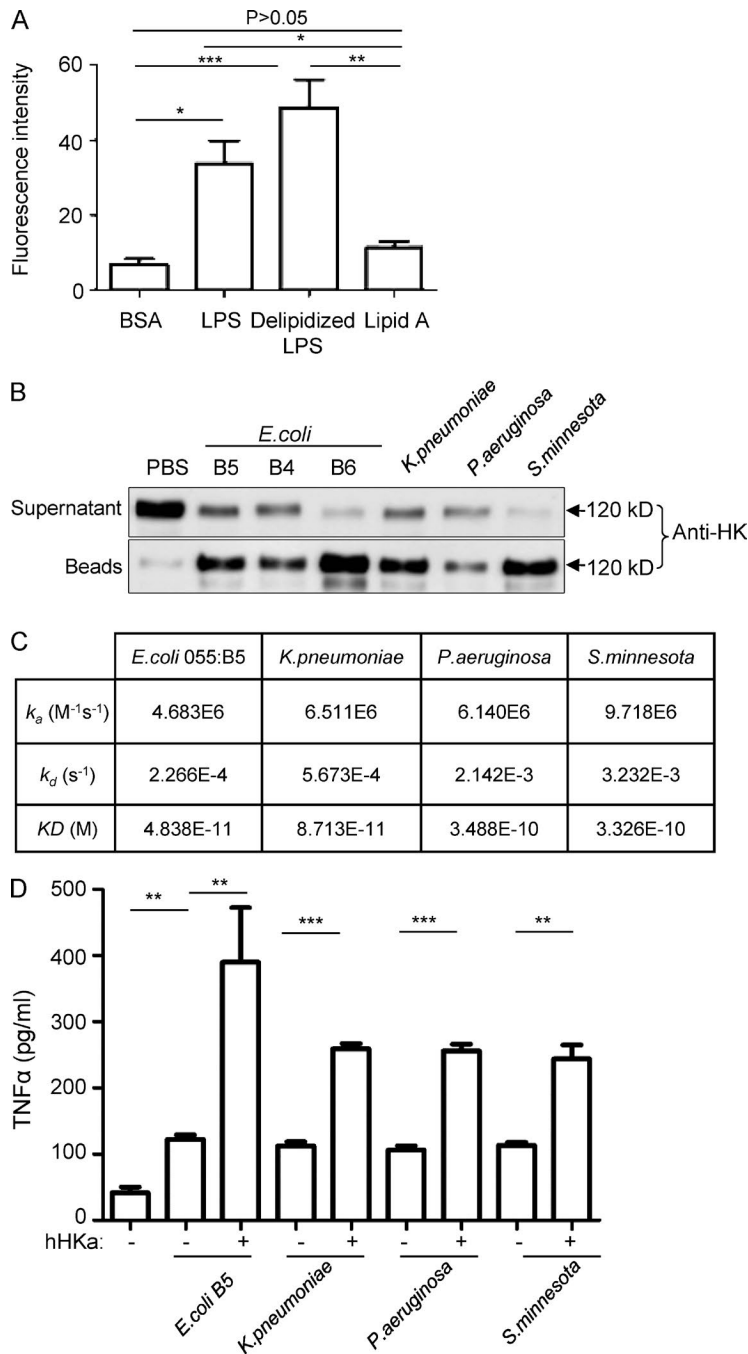
Figure 7. **HK associates with different LPS species.** (A) Microtiter plate wells were coated with BSA, LPS, delipidized LPS, or lipid A at 2 µg/well. The wells were incubated with 100 nM FITC-HK for 1 h. After washing, the bound FITC-HK was quantified using SpectraMax M5. Statistics were analyzed using an ANOVA. *, P < 0.05; **, P < 0.01; ***, P < 0.001. Data are representative of two independent experiments and expressed as mean ± SEM. (B) 10 µg/ml human HK was incubated with 10 µg/ml LPS from the different sources indicated for 30 min, followed by incubation with polymyxin B beads. HK associated with beads, and in the postincubation solution, was detected by immunoblotting with an anti-HK antibody. Data are representative of two independent experiments. (C) SPR analyses of the binding of LPS from different bacteria to HKa. An HKa solution was passed over the hydrophobic HPA sensor chip that had been immobilized with one of three types of LPS isolated from *K. pneumoniae*, *P. aeruginosa*, and *S. minnesota* and one type of LPS from *E. coli* 055:B5. An activated/deactivated flow cell was used to evaluate nonspecific binding. Data are representative of two independent experiments. (D) Raw 264.7 cells (2.5 × 10⁶ cells/ml) were incubated with, or without, human HKa in the presence or absence of 0.03 ng/ml different species of LPS in serum-free DMEM at 37°C for 6 h. The concentration of TNF in the culture supernatants was determined using ELISA. Statistics were analyzed using ANOVA. **, P < 0.01; ***, P < 0.001. Data are representative of two independent experiments and expressed as mean ± SEM.

confirmed the expected lack of immunoreactivity with the HK/Δ492-506 protein (Fig. S5 C). Using the experimental method described in Fig. 4 B, reconstitution of $Kng1^{-/-}$ mice with HK/Δ492-506 did not lead to a recovery in circulating LPS to the levels of WT mice (Fig. S5 D), which is in contrast to the effect of the normal HK protein (Fig. 4 B). This observation supports the notion that the DHG15 region of HK is critical for endotoxemia. Plasma BK levels in $Kng1^{-/-}$ mice were, however, increased by reconstitution with HK/Δ492-506 (Fig. S5 E). The in-

consistency between recovery of BK levels and recovery of LPS levels by HK/Δ492-506 suggests that the DHG15 region of HK is not involved in LPS–induced BK production but is important in the maintenance of circulating LPS levels. Other pathways that are independent of HK-LPS binding have been shown to contribute to BK production. For example, LPS stimulates neutrophils to release elastase, cathepsins, and protease-3, all of which can cleave HK to release BK (Wu, 2015), without the requirement of a direct HK-LPS interaction. The levels of plasma BK recovered in
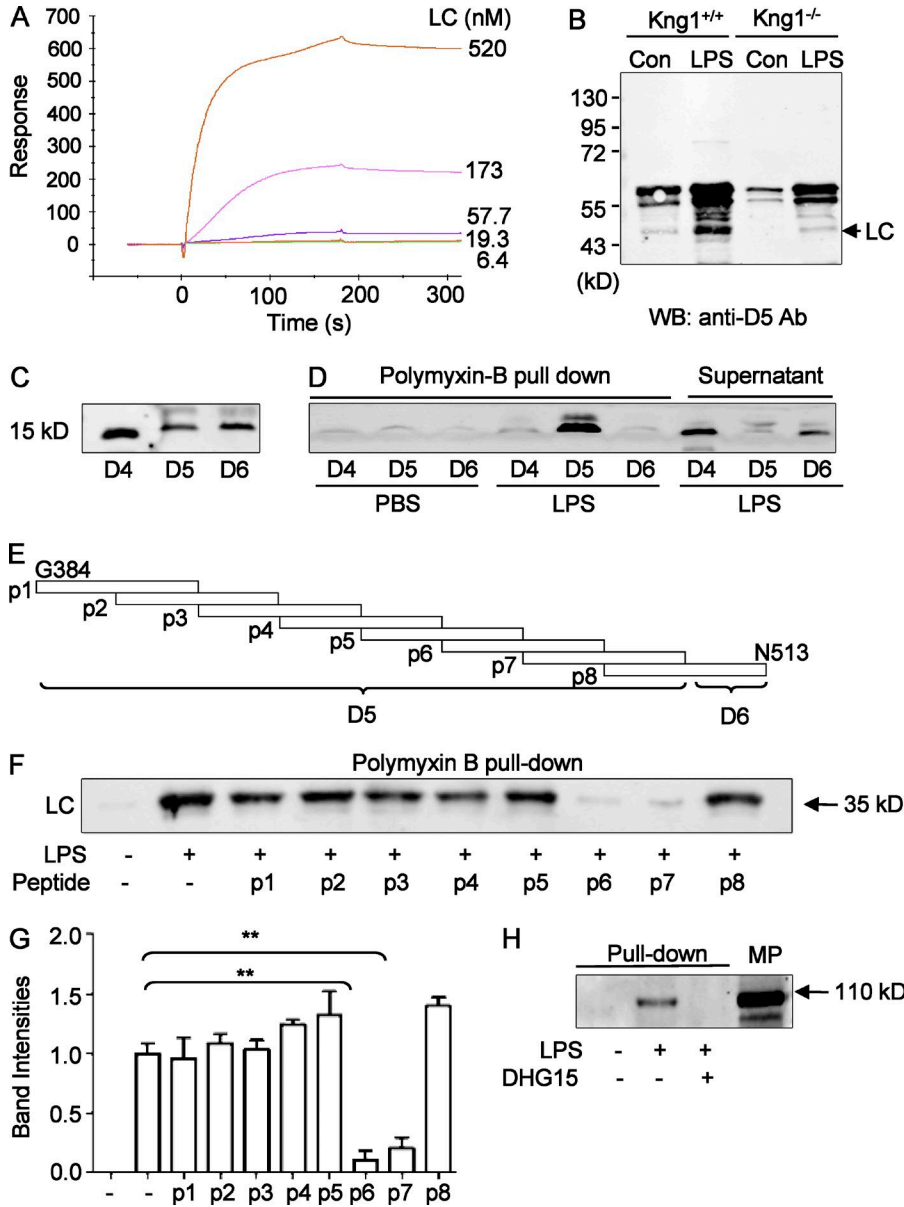
Figure 8. **The DHG15 region in D5 is the site of HK responsible for LPS binding.** (A) Analysis of LC binding to LPS using SPR assay showing a K_d of 1.52×10^{-9} M. One representative experiment out of three independent experiments is shown. (B) LC is released from LPS-treated plasma and forms a complex with LPS. Plasma (200 µl, diluted 1:1 with PBS) from WT mice and $Kng1^{-/-}$ mice was incubated with either 40 µl control Sepharose beads or LPS-conjugated Sepharose beads at room temperature for 2 h. After washing, proteins associated with the beads were analyzed by immunoblotting using an anti-D5 of HK antibody. Data are representative of two independent experiments. (C) Recombinant D4, D5, and D6 domains from HK-LC generated from Sf9 insect cells analyzed by anti-His immunoblotting (left). (D) The recombinant D4, D5, and D6 domains (10 µg/ml) were incubated in a volume of 200 µl with either PBS or LPS (25 µg/ml), respectively, followed by incubation with polymyxin B beads. The bead-associated proteins were then analyzed by anti-His immunoblotting. Data are representative of three independent experiments. (E) The indicated variety of 30-mer peptides (p1–p8) derived from the D5 and D6 domains were synthesized. (F) 25 µg/ml LPS was preincubated with peptides p1–p8 (50 µg/ml), followed by incubation with 10 µg/ml HK-LC. After pull-down with polymyxin B beads, the bead-associated proteins were analyzed by anti-His immunoblotting. The experiments were performed in triplicate, and the band density of LC was quantitated (G). Data were analyzed using an unpaired Student's t test and are representative of two independent experiments. **, P < 0.01. Data are expressed as mean ± SEM. (H) As indicated, 40 µl LPS-conjugated Sepharose beads were preincubated with, or without, 100 µg/ml DHG15 peptide, followed by incubation with 100 µl of mouse plasma at room temperature for 2 h. The beads were then washed three times with PBS containing 0.1% Triton X-100, and the proteins associated with beads were subjected to SDS-PAGE and immunoblotting with an anti-HK antibody. Data are representative of three independent experiments.

$Kng1^{-/-}$ mice by HK/Δ492-506 were not as high as those of WT mice (Fig. S5 E), which is probably due to their decrease in circulating LPS levels with less stimulation of other pathways for HK cleavage (Fig. S5 D).

mAb against the D5 of HK (C11C1) ameliorates LPS–induced systemic inflammation

We have previously characterized C11C1 as a specific inhibitory mAb raised against the D5 domain of HK (Song et al., 2004; Khan et al., 2010). As shown in Fig. 9 A, C11C1 recognized only mouse single-chain HK (SCHK) but not the ΔmHK-D5 and LK. Furthermore, this antibody was confirmed to recognize purified HK and HKa, recombinant proteins of LC and D5 in immunoblotting (Fig. 9 B). Moreover, when C11C1 was preincubated with mouse plasma, it blocked mouse HK binding to LPS (Fig. 9 C). Thus, we tested the effect of C11C1 on endotoxemia in vivo. Treatment with C11C1 significantly in-
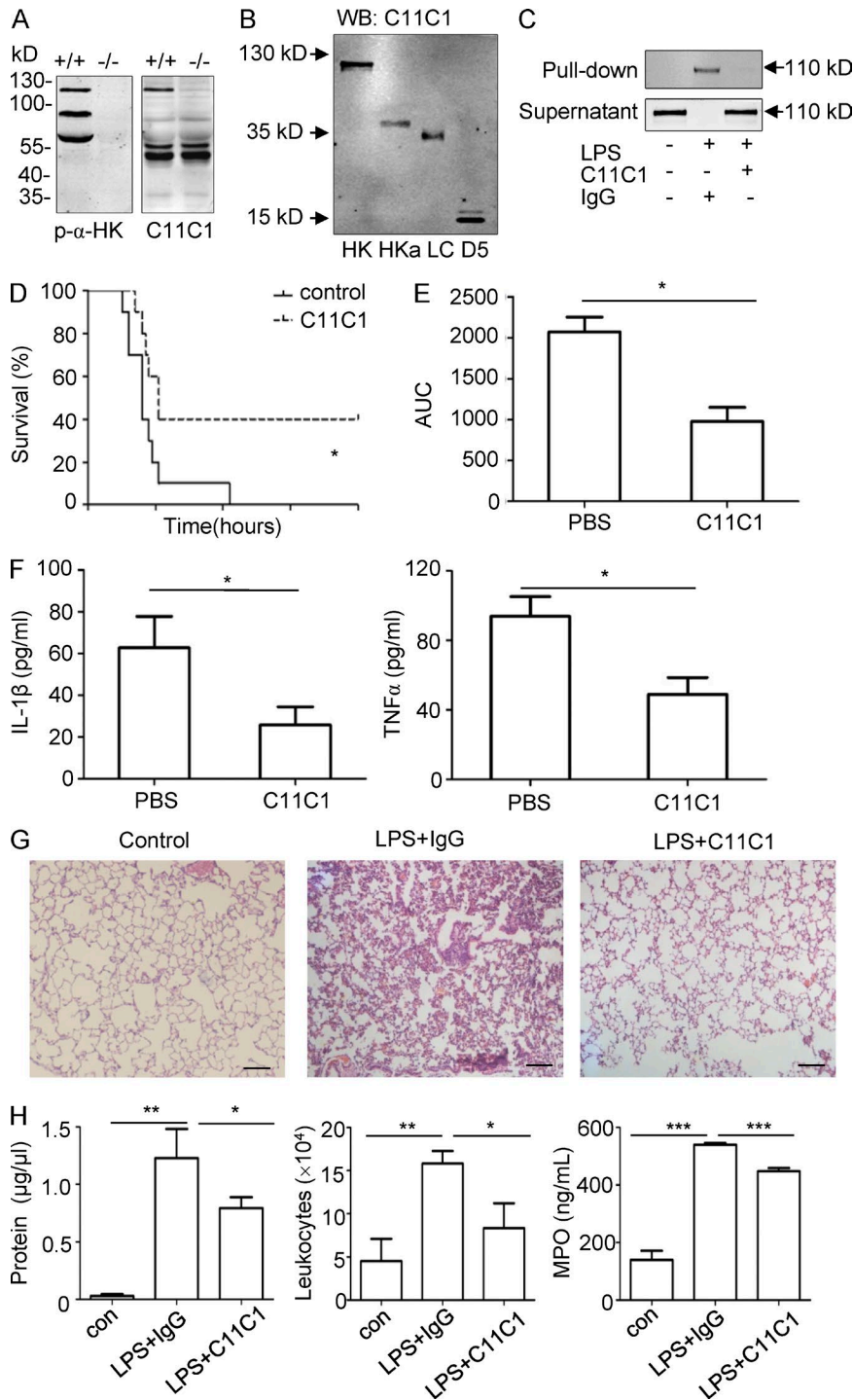
Figure 9. **The mAb C11C1 against the D5 domain from HK significantly suppresses LPS–induced systemic inflammation in WT mice.** (A) Plasma from WT (+/+) mice and Kng1$^{-/-}$ (−/−) mice was separated by SDS-PAGE and analyzed by immunoblotting using either a polyclonal anti-HK Ab (left) or the monoclonal C11C1 antibody (right), respectively. (B) 50 ng HK, HKa, LC, or D5 was separated by SDS-PAGE and detected by immunoblotting using the C11C1 mAb. (C) Diluted mouse plasma was preincubated with 30 µg/ml of C11C,1 or an isotype control mouse IgG, followed by incubation with 20 µg/ml of LPS. LPS and its associated proteins were then pull-downed using polymyxin B beads. The proteins associated with the beads and remaining in the supernatant were analyzed by immunoblotting with the C11C1 mAb. Data are representative of three independent experiments. (D) Two groups of 8-wk-old WT C57BL/6 mice ($n = 12$) received an i.v. injection of mouse IgG (mIgG) or C11C1 antibody at 40 mg/kg. After 15 min, both groups of mice received an i.p. injection of LPS (25 mg/kg), and the survival rate was monitored. Data were analyzed using a log-rank test and are representative of two independent experiments. *, $P < 0.05$. (E and F) Two groups of WT C57BL/6 mice ($n = 8$) received an injection of mIgG or C11C1 antibody at 40 mg/kg before receiving an i.p. injection of 5 mg/kg of LPS. Blood was collected at 0, 3, 6, 12, and 24 h after LPS injection, and the endotoxin kinetics were measured and the AUC was calculated. The levels of IL-1β and TNF in blood collected at 6 h were measured by ELISA (F). Data were analyzed using an unpaired Student's t test and are representative of two independent experiments. *, $P < 0.05$. Data are expressed as mean ± SEM. (G) 24 h after LPS challenge, the lung was removed, fixed, and stained with hematoxylin and eosin stain, and the images are shown. Bars, 100 µm. (H) 24 h after LPS challenge, BALF was collected and its total protein concentration and white blood cell content were determined. The MPO activity in the lung homogenate was also measured. Statistics were analyzed using an ANOVA. *, $P < 0.05$; **, $P < 0.01$; ***, $P < 0.001$. Data are representative of two independent experiments and expressed as mean ± SEM.

creased the survival rate of WT mice challenged with a lethal dose of LPS (Fig. 9 D). Consistent with this, C11C1 significantly reduced the total kinetic circulating LPS levels (area under the curve) in WT mice (Fig. 9 E) and the production of IL-1β and TNF in circulation (Fig. 9 F). In addition, C11C1 attenuated the infiltration of leukocytes into the lungs as indicated by hematoxylin and eosin staining (Fig. 9 G) and reduced the total leukocyte number and protein levels in BALF, as well as the MPO levels in lung homogenates (Fig. 9 H). These data suggest that the interaction between HK and LPS is a target with a therapeutic potential in the treatment of endotoxemia.

Human HKa and mouse HKa display similar activities in their interaction with LPS

Humans are very sensitive to LPS toxicity, whereas rodents are resistant. Because HK binds LPS in both human and murine plasma (Figs. 5, 7, 8, and 9), we investigated whether human HK and mouse HK have different activities with regard to their interaction with LPS. In a disaggregation assay, human HKa and mouse HKa had a similar ability to disaggregate LPS (Fig. 10 A). When incubated with monocytes, both human HKa and mouse HKa enhanced LPS-stimulated TNF to comparable extents (Fig. 10 B). It is known that mice have two SCHK species, namely, a single-chain form of HK (SCHK; 110 kD) and ΔmHK-D5 (82 kD; Fig. S1 F; (Merkulov et al., 2008), whereas humans only have one SCHK. We found that the anti-DHG15 antibody only recognized human HK and mouse HK of 110 kD (SCHK), but not mouse ΔmHK-D5 (82 kD; Fig. 10C), suggesting that human SCHK (hSCHK) and mouse SCHK (mSCHK) are selective for binding LPS. Interestingly, in immunoblots using the anti-DHG15 antibody, the band intensity of hSCHK/120 kD was much higher than that of mSCHK/110 kD (Fig. 10 C), suggesting that the level of hSCHK/120 kD is much higher than the level of mSCHK/110 kD. To quantify the concentrations of SCHK in plasma, we used the immunoblotting method described by Reddigari and Kaplan (1989). In brief, 5–160 ng purified hSCHK was added to 1 μl kininogen-deficient human plasma and electrophoresed under nonreducing conditions and immunoblotted (Fig. 10 D). When the band intensities were plotted against the nanogram amount of hSCHK applied to the gel, a straight line was obtained (Fig. 10 D, top). When normal human plasma was included on the same gel as purified hSCHK and quantified, it was found that plasma contained 86.83 ± 2.45 μg/ml hSCHK (Fig. 10 D). Using the same method, we quantified the level of mSCHK/110 kD in mouse plasma and found it to be 39.56 ± 4.87 μg/ml (Fig. 10 D, bottom). Although the low concentration of LPS-binding SCHK in mouse plasma may explain their reduced sensitivity to LPS compared with humans, the exact contribution of HK to the different response of human and mice to LPS awaits further verification using a humanized mouse model.

DISCUSSION

The correlation of elevated circulating endotoxin levels with adverse outcomes in critically ill patients with sepsis suggests that endotoxin clearance is compromised. Because LPS is not in a free form in circulation, the identification of the major plasma protein supporting LPS levels in circulations is very important. In this study, we provide the first genetic evidence showing the important role of HK in the pathogenesis of endotoxemia. Mice lacking HK are protected against LPS-induced mortality, and both mice and rats lacking HK have reduced circulating LPS levels, demonstrating that the role of HK in LPS-induced mortality is associated with the circulating LPS levels. Replenishment of HK-deficient mice with human HK increases the LPS levels and renders them susceptible to the LPS response. These in vivo observations indicate that the role of HK in the LPS-induced inflammatory response is highly evolutionarily conserved. In plasma, LPS induces HK cleavage to produce the two-chain HKa, containing one HC and one LC. Both HKa and the LC could disaggregate LPS, and in addition, the LC potentiates LPS-induced TNF production from myeloid cells. Compared with HK, the LC binds to LPS with a higher affinity ($K_d = 1.71 \times 10^{-7}$ M vs. 1.52×10^{-9} M). The binding site on HK for LPS is located at the DHG15 (DHGHKHKHGHGH GKH) amino acid region of the D5 domain in the LC. Importantly, from a therapeutic perspective, an anti-D5 mAb significantly ameliorates LPS-induced inflammation and reduces circulating LPS levels in WT mice. Thus, to the best of our knowledge, HK is the most important LPS carrier supporting endotoxemia and is essential for LPS-induced inflammation.

It has been known for a long time that the CD14–MD-2–TLR4 pathway is critical for LPS-induced septic shock, because mice lacking CD14, MD-2, and TLR4 are resistant to a lethal dose of LPS (Park and Lee, 2013). In contrast, mice lacking LBP, the major LPS-binding protein identified to date, remain sensitive to LPS-induced mortality (Wurfel et al., 1997), suggesting the existence of an LBP-independent pathway. In this study, we found that HK-deficient mice share the same phenotype with mice lacking CD14, MD-2, and TLR4, having resistance to LPS-induced mortality, revealing that HK constitutes an essential element component of the CD14–MD-2–TLR4 pathway. In contrast to the role of CD14–MD-2–TLR4 in the cellular response to LPS, the main function of HK appears to be to serve as an LPS carrier to allow LPS persistence in circulation, thereby amplifying the host response to LPS. HK could thus be beneficial for the host as a triggering signal in the presence of low concentrations of LPS but detrimental in the presence of higher concentrations of LPS. Efficient endotoxin clearance from circulation prevents excessive or unwanted inflammation in response to LPS during a gram-negative infection; however, numerous large clinical trials assessing a range of anti-endotoxin therapies have failed without an adequate explanation. Our finding that HK serves as the major LPS carrier that prevents LPS clearance underlies the insufficiency of current anti-endotoxin therapies. In this regard, encouragingly, blockade of the LPS-HK interaction using the C11C1 mAb significantly suppressed LPS-induced systemic inflammation and circulating LPS levels. Thus, our findings provide a new avenue to facilitate LPS clearance, thereby shifting the current paradigm of anti-endotoxin strategies: blocking LPS binding to host protein.

Although the involvement of the KKS in patients with endotoxemia and sepsis has been known for three decades (Wu, 2015), its pathological role has never been characterized. Consequently, neither the way in which the KKS participates in these processes nor the mechanisms that trigger its activation are understood. In this study, we evaluated the role of the KKS in sepsis using a group of KKS-knockout mice,
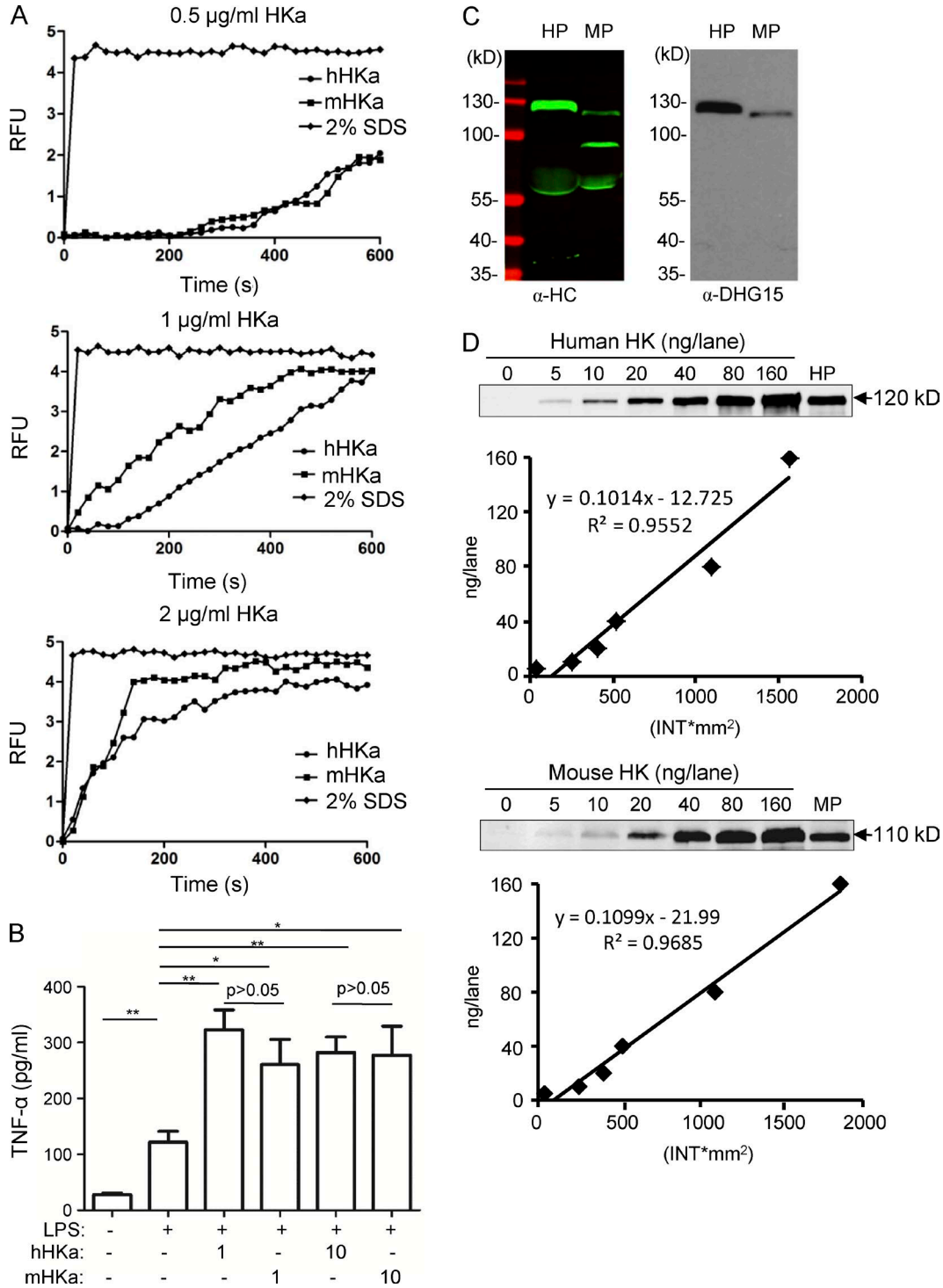
Figure 10. **Comparison of human HK and mouse HK in their interaction with LPS.** (A) BODIPY FL–LPS at 50 ng/ml was suspended in 100 µl PBS. After the addition of human HKa or mouse HKa at the indicated concentrations, the real-time change in BODIPY FL–LPS fluorescence upon transition from the aggregated LPS state was recorded in 20-s intervals. Data are representative of two independent experiments. (B) Raw 264.7 cells were incubated with, or without, human HKa or mouse HKa (µg/ml) in the presence or absence of 0.03 ng/ml LPS at 37°C for 6 h. The concentration of TNF in the culture supernatants was determined using ELISA. Statistics were analyzed using an ANOVA. *, P < 0.05; **, P < 0.01. Data are representative of two independent experiments and expressed as mean ± SEM. (C) 1 µl human or mouse plasma was solubilized in SDS sample buffer and separated by SDS-PAGE. The samples were analyzed by immunoblotting using a polyclonal anti–HK-HC antibody (left) or an anti-DHG15 antibody (right). (D) Quantification of human SCHK and mouse SCHK in plasma by immunoblotting. 1 µl kininogen-deficient human plasma supplemented with 0, 5, 10, 20, 40, 80, or 160 ng human SCHK and

providing the first evidence showing that HK is essential in LPS–induced mortality, but other components of the KKS are dispensable (Fig. 1). Our observation is consistent with evolutionary analysis along mammalian phylogeny showing no evidence of adaptive evolution for FXII and pKal but instead a strong signature of diversifying positive selection detected for HK (Cagliani et al., 2013). Previous studies have shown that the chicken and jawless fish genomes have a gene for kininogen but do not possess the FXII gene (Kos et al., 1992; Zhou et al., 2008; Doolittle, 2011). Birds have a kininogen composed of three cystatin domains, a BK domain, a histidine-rich domain, and a carboxyl-terminal domain (Doolittle, 2011). Presumably, kininogen is also involved in the response of birds and jawless fish to LPS, and the role of kininogen in the host response to LPS is likely an evolutionarily conserved function.

Recent studies have shown that kininogen has pathological functions. For example, kininogen deficiency protects from thrombosis, blood–brain barrier damage, and inflammation by proteolytic BK formation and defective fibrin formation (Merkulov et al., 2008; Langhauser et al., 2012; Fang et al., 2013). However, this new function for kininogen in supporting circulating LPS level is independent of LPS–induced proteolytic pathways, because dual deficiency of two BK receptors did not protect mice against LPS–induced lethality (Fig. 1). The identification and characterization of the role of HK in endotoxemia using genetically modified models provides a precise evaluation of the role of the KKS in sepsis and will help develop new HK-targeting approaches. Moreover, because of the broad involvement of LPS in a variety of pathological processes, the role of HK in LPS biology will facilitate our studies into the function of HK in various LPS-driven disorders, such as metabolic endotoxemia, atherosclerosis, and insulin resistance.

Recently we have shown that HK binds to phosphatidylserine (PS), resulting in its cleavage to HKa, which can bind PS with a higher binding affinity than HK (Yang et al., 2014). Both PS and LPS contain negative charges; here, we found that HK has the same capacity in binding to LPS. The HK in whole blood challenged with LPS was also cleaved into HKa, as indicated by the release of LC (Fig. 8). Through this dynamic change, HKa gained a potent ability to disaggregate LPS, probably through a conformational change that exposed its LC. This tightly regulated process underlies the essential role of HK in the maintenance of circulating LPS levels. Its binding to LPS may prevent the binding of LPS to other LBPs in circulation such as lipoproteins, thereby delaying the processes of LPS metabolism and clearance. Whether and how HK competes with these other LBPs need further investigation. In addition to a higher binding affinity for LPS, the LC of HK amplified LPS-stimulated TNF production (Fig. 7), indicating an additional effect of HK in LPS biology. Interestingly, we found that HK is able to bind various LPS species, consistent with its binding to LPS via the carbohydrate region, but not lipid A (Fig. 7). These observations suggest that HK is a general regulator of LPS. Similarly, other proteins such as BAI1 also bind the outer carbohydrate-rich structures of LPS, and not lipid A (Das et al., 2011).

In summary, our findings demonstrate that HK is an essential LPS carrier for endotoxemia and can disaggregate LPS and amplify the response of immune cells. These multifaceted properties of HK provide novel insights into the complex interaction between LPS and host recognition machinery. The identification of the molecular mechanisms by which HK governs the circulating LPS concentration is of extreme importance, as it in turn reveals HK to be a new anti-endotoxin target for promoting LPS clearance and improving outcomes in patients with sepsis.

MATERIALS AND METHODS
Materials

LPS from *E. coli* including 055:B5 (B5), 0111:B4 (B4), 026:B6 (B6), *K. pneumoniae*, *P. aeruginosa*, and *S. minnesota*, delipidized LPS, lipid A, cyanogen bromide (CNBr)–activated resin, D-galactosamine, polyinosinic:polycytidylic acid, control mouse IgG, and the FITC labeling kit were purchased from Sigma-Aldrich. BODIPY FL–conjugated *E. coli* 055:B5 LPS and BODIPY FL dye were from Molecular Probes. Endotoxin-free murine TNF and ELISA kits for mouse TNF, IL-1β, IL-6, HMGB-1, and MPO were from R&D Systems. The BK ELISA kit and chromogenic LAL endotoxin kit were from Enzo Life Sciences. Polymyxin B-Separopore (Agarose) 4B-CL beads (Affisorbent Endotoxin Removal Gel) was from BioWorld. Allophycocyanin (APC)-conjugated anti-CD11b and PE-labeled antibodies, including anti-CD90, anti-B220, anti-CD49b, anti-NK1.1, and anti-Ly6G, were from eBioscience. Polyclonal antibodies against HK–HC and His-tag were from Abgent. Rabbit polyclonal anti-HK D5 was generated by GenScript. The anti-FXII antibody was from Santa Cruz Biotechnology. IRDye 800–conjugated goat anti-mouse IgG and IRDye 680–conjugated goat anti-rabbit IgG were from LI-COR Bioscience. Recombinant human HK and HKa, and mouse HK and HKa were purchased from Bio-Techne. Human plasma depleted for kininogen by immunoaffinity chromatography (kininogen-deficient plasma) was from Sekisui Diagnostics.

---

1 µl fresh human plasma were electrophoresed and immunoblotted using an anti-DHG15 antibody (top). Similarly, 1 µl kininogen-deficient mouse plasma supplemented with 0, 5, 10, 20, 40, 80, or 160 ng of mouse SCHK and 1 µl fresh WT mouse plasma were electrophoresed and immunoblotted using an anti-DHG15 antibody (bottom). The intensity of bands in the immunoblots were analyzed as described in Materials and methods. A standard curve for protein concentration was created by plotting intensity as a function of protein quantity. The quantification was performed using three samples of human plasma and four samples of mouse plasma. Data are representative of two independent experiments. RFU, relative fluorescence units.

Animals

Generation of Kng1⁻/⁻ mice. In mice, plasma HK is encoded by the *Kng1* gene (Gene ID: 16644) which is localized on chromosome 16: 23,058,421–23,081,759. This gene is expressed in liver, where HK is produced, and then secreted into the circulation. To generate a *Kng1*-knockout strain, a knock-out-targeting vector was constructed by replacing exon 2 and exon 3 of the Kng1 gene with a PGK–Neo cassette in a 9-kb genomic fragment of BAC clone bMQ-175I03 vector. The vector with this cassette was introduced into EL350 cells, and recombination induced between the homologous sequences resulted in replacement of *Kng1* exons 2 and 3 with the loxP-PGK-Neo-loxP sequence. After positive ES cells were verified by Southern blot hybridization, a total of 20 clonal ES cells containing the disrupted *Kng1* exons 2 and 3 were injected using blunt-tipped pipettes and a Leitz manipulation system into 3.5-d sv129 mouse blastocysts, which were then implanted into 2.5-d CD1 pseudo-pregnant recipients by uterine transfer. The degree of chimerism in the offspring was assessed 2 weeks after birth by identification of agouti coat color. Strong chimeras were tested for germline transmission by crossing with C57BL/6J mice. The offspring were tested for transmission of the targeted floxed allele. The floxed mice were then mated with CMV-Cre mice to generate conventional knockouts. Homozygous null offspring were produced by intercrossing heterozygotes. The sequence of primers used for genotyping by PCR were as follows: primer 1: 5′-CAGGGTTTTACCTCACCTTAGGTC-3′; primer 2: 5′-TAGCTGGGCAGAAGGTACATAG-3′; primer 3: 5′-CGTGTGTGATTCAGAAGGTGAAG-3′; Neo-3F: 5′-TCTGAGGCGGAAAGAACCAG-3′; Cre-F: 5′-GCGGTCTGGCAGTAAAAACTATC-3′; Cre-R: 5′-GTGAAACAGCATTGCTGTCACTT-3′.

Double-knockout mice lacking both BK receptors (B1RB2R⁻/⁻) mice and TLR4⁻/⁻ knockout mice were purchased from Jackson Laboratories. Mice lacking pKal (Klkb1⁻/⁻ mice) and mice lacking factor XII (FXII⁻/⁻ mice) were provided by Dr. E. Feener (Harvard University) and Dr. F. Castellino (University of Notre Dame), respectively. In in vivo experiments, all knockout mice, including Kng1⁻/⁻ mice, were backcrossed onto a C57BL/6 background for more than 10 generations, and their littermates were used as controls. HK–deficient Brown Norway rats were provided by Dr. Elena Kaschina (Charite University), and WT Brown Norway rats purchased from Charles River Laboratories were used as controls. Experiments with mice and rats were performed in accordance with protocols approved by the Institutional Animal Care and Use Committees of Soochow University and Temple University.

Expression of Kng1 and Kng2 mRNA in mouse liver and HK protein in plasma

To analyze the expression levels of Kng1 and Kng2 mRNA, total RNA was isolated from murine liver using TRIzol (Invitrogen) and reverse-transcribed to cDNA using Moloney murine leukemia virus polymerase. The first-strand reaction was amplified by PCR using primers spanning Kng1 exon 2 and exon 3 as follows: 5′-CAAGTATCTAATCAAGGAGGGC-3′ (forward) and 5′-CAGGTCTGGGTGACTATGAAG-3′ (reverse). The PCR primers used to examine Kng2 expression were 5′-AATCAAGGAGGGCAACTGCT-3′ (forward) and 5′-CCTTCGGATAGGAATAGTCTTAC-3′ (reverse). The primer pair used to examine the expression of β–actin mRNA (control) was 5′-GTCCCTCACCCTCCCAAAAG-3′ (forward) and 5′-GCTGCCTCAACACCTCAACCC-3′ (reverse). The PCR products were visualized by electrophoresis on a 2% agarose gel. The level of HK in mouse plasma was detected by immunoblotting using an anti–HK antibody.

Endotoxemia model

In this study, heterozygous knockout mice were mated, and their homozygous knockout offspring and their WT littermates were used in the experiments at 8 wk of age. LPS was injected i.p. at the indicated doses, followed by an observation of survival and inflammatory analysis as previously described (Wang et al., 2009).

Measurement of BK levels in plasma

As previously described, whole blood was collected by cardiac puncture. Immediately after separation of plasma by centrifugation, the levels of BK were measured (Dai et al., 2012).

Histology

Tissues were dehydrated and then embedded in paraffin. After removal of the paraffin, the tissues were then stained with hematoxylin and eosin (Dai et al., 2012) before viewing with a Leica DM2000 microscope. For electron microscopy, lung samples from the mice were fixed as previously described (Herwald et al., 2003; Oehmcke et al., 2009). The fixed samples were washed, dehydrated, critical point dried, and sputtered with palladium/gold (Herwald et al., 2003). Specimens were examined using a scanning electron microscope (Philips Electronic xl–20) operated at an acceleration voltage of 5 kV. Images were captured using a Satan Multiscan 791 charge-coupled device camera.

Quantification of inflammatory cells and proteins in BALF

As previously described, the trachea was exposed and connected to a syringe filled with 1 ml isotonic PBS (Håkansson et al., 2012; Grailer et al., 2014). The airways were manually perfused, and BALF was harvested by slow instillation and retraction. The BALF was then centrifuged at 300 *g* for 10 min, and the supernatant and cell pellet were collected. The number of leukocytes in the pellet was counted using an automated hematology analyzer (KX-21N; Sysmex Corporation; Moon et al., 2012). BALF was stored at −80°C until use. The concentration of protein in the supernatant was measured using the bicinchoninic acid method. Lung tissues were homogenized, and the ho-

mogenate was centrifuged at 5,000 g for 5 min. The concentration of MPO in the lung homogenate was assayed using a mouse MPO ELISA kit.

Flow cytometric analysis

The cells were washed twice, and 10^6 cells were suspended in 50 µl PBS supplemented with 1% FBS and stained for 20 min at 4°C with fluorescently conjugated antibodies (1:500), including FITC–conjugated anti-Ly6C, CD115, B220, CD3e, and Ly6G antibodies (eBioscience). Stained cells were then analyzed using a FACSCanto flow cytometer using FAC SDiva software (BD Biosciences), and the data were analyzed using FlowJo software (TreeStar).

Measure of endotoxin levels in plasma

Blood was collected from the tail vein, and plasma endotoxin levels were measured using the chromogenic LAL detection method (Khan et al., 2006; Champion et al., 2013; Pais de Barros et al., 2015).

Isolation of PBMCs and monocytes from mice

Mouse blood was drawn via cardiac puncture into a syringe with heparin as an anticoagulant. Blood was diluted (1:1) with Dulbecco's PBS without calcium and magnesium. The diluted samples were subjected to density gradient separation on Histopaque-1083 (ratio 1:1; Sigma-Aldrich) and centrifuged. The PBMC layer was collected and washed in HBSS with phenol red without calcium and magnesium (Lonza).

Mouse monocytes are defined as CD11b^{high} (CD90/B220/CD49b/NK1.1/Ly6G/Ter-119)^{low}. To purify monocytes, whole blood was incubated with a mix of different antibodies (PE-labeled CD90, B220, CD49b, NK1.1, Ly6G, Ter-119, and APC-labeled CD11b; Zhou et al., 2015). After dilution with one volume of sorting buffer, the samples were transferred onto Histopaque in a FACS tube. After centrifugation at 300 g for 10 min, the interphase containing mononuclear cells was collected and then diluted with one volume of sorting buffer containing 2% serum and 2 mM EDTA. The labeled mononuclear cells were sorted using a BD FAC SAria II (BD Biosciences).

Measurement of monocytic cytokine mRNA levels by quantitative RT–PCR assay

The levels of cytokine RNA expression in white blood cells and monocytes were quantitated using an ABI 7500 system (Applied Biosystems; Xie et al., 2014). The sequence of the primers used was as follows: TNF-F: 5′-CTACTCCCAGGT TCTCTTCAA-3′; TNF-R: 5′-GCAGAGAGGAGGAGG TTGACTTTC-3′; IL-1β-F: 5′-TGTGTCTTTCCCGTG GACCT-3′; IL-1β-R: 5′-CAGCTCATATGGGTCCGA CA-3′; IL-6-F: 5′-GGTGACAACCACGGCCTTCCC-3′; IL-6-R: 5′-AAGCCTCCGACTTGTGAAGTGGT-3′; actin-F: 5′-GTGCTATGT TGCTCTAGACTTCG-3′; actin-R: 5′-ATGCCACAGGATTCCATACC-3′.

Cell culture

RAW 264.7 cells (ATCC TIB-71), a mouse monocyte/macrophage-like cell line, were cultured in DMEM supplemented with 2 mM glutamine and 10% heat-inactivated FBS (Hyclone).

SPR assay

A Biacore 3000 biosensor instrument (GE Healthcare) was used to measure the interaction between LPS and HK (Hyakushima et al., 2004; Wang et al., 2009). In brief, LPS diluted with running buffer (10 mM Hepes, 100 mM NaCl, pH 7.4) was immobilized on a HPA sensor chip (GE Healthcare). Different concentrations of HK and its LC were injected into the flow cells at a rate of 10 µl/min, and the sensorgram and relative response units (RU) for interaction to LPS were monitored for 5 min. The sensor surface was then washed with the same buffer to initiate dissociation, and the chip was finally regenerated with 50 mM NaOH at a flow rate of 50 µl/min. Differences in RU were recorded after subtraction of the response in the reference cell that was activated and deactivated in an identical way. A saturation-binding curve was depicted as a function of HK concentration versus RU. The dissociation constant of LPS (K_d) was calculated as the ratio of two constants (k_{off}/k_{on}).

Generation of HK domains and synthetic peptides

The recombinant proteins HK-HC (Q19-K389), HK-LC (S390-S644), HK-D4 (376I-401T), HK-D5 (402V-520K), and HK-D6 (521T-644S) containing a C-terminal His tag were generated using the Bac-to-Bac baculovirus expression system. Baculovirus at a multiplicity of infection of 3 was used for infection of Sf9 insect cells (Lin et al., 2014). After infection for 72 h, supernatants were harvested and subjected to three freezing and thawing cycles. Clear supernatants were centrifuged at 10,000 g for 30 min to spin down large protein complexes or baculovirus particles. Proteins present in the supernatant were purified by Ni-Sepharose 6 Fast Flow column (GE Healthcare). The following peptides were commercially synthesized by GenScript: VSP PHTSMAPAQDEERDSGKEQGHTRRHDW (peptide 1), RDSGKEQGHTRRHDWGHEKQRKHNLGHGHK (peptide 2), GHEKQRKHNLGHGHKHERDQGHGH QRGHGL (peptide 3), HERDQGHGHQRGHGLGHG HEQQHGLGHGHK (peptide 4), GHGHEQQHGLGH GHKFKLDDDLEHQGGHVL (peptide 5), FKLDDD LEHQGGHVLDHGHKHKHGHGHGKH (peptide 6), DHGHKHKHGHGHGKHKNKGKKNGKHNGWK (peptide 7), and KNKGKKNGKHNGWKTEHLASSSED STTPS (peptide 8). Peptides 1–7 were derived from the D5 domain of HK, and peptide 8 was derived from the N terminus of the D6 domain.

Recombinant human HK lacking 492–506 (DHGHKH KHGHGHGKH; HK/Δ492-506) was generated by GenScript using a mammalian expression system. The plasmid expressing HK/Δ492-506 with a C-terminal 10× His tag was transfected into Expi293F cells (Thermo Fisher Scientific). Expi293F cells were grown in serum-free Expi293F™ Ex-

pression Medium (Thermo Fisher Scientific) in Erlenmeyer flasks (Corning) at 37°C with 8% CO_2 on an orbital shaker (VWR Scientific). Protein was obtained from the cell culture supernatant and purified using HisTrap FF Crude. The protein purity, size, and identity were verified by Coomassie brilliant blue staining and immunoblotting using a mouse anti-His antibody (catalog no. A00186; GenScript) with the use of a positive control Multiple-tag (catalog no. M0101; GenScript) and protein markers (catalog no. MM0908; GenScript).

Analysis of LPS–associated proteins by pull–down assay
To generate LPS–conjugated CNBr-activated Sepharose beads, LPS in 0.1 M $NaHCO_3$ buffer containing 0.5 M NaCl, pH 8.4, was incubated with Sepharose beads at 2–8°C overnight (Baik et al., 2013). Unreacted groups were blocked with 1 M ethanolamine, followed by extensive washing. In some experiments, polymyxin B–agarose beads were also used. Proteins and recombinant domains were incubated with LPS–conjugated CNBr-activated Sepharose beads, or with LPS and subsequent addition of polymyxin B beads. The beads were washed twice with PBS and analyzed by immunoblotting.

Western blotting
Samples were solubilized in buffer (25 mM Tris, pH 7.4, 150 mM NaCl, 1% NP-40) containing 0.1% SDS and 4% proteinase inhibitor (complete protease inhibitor cocktail; Roche) and treated with 4× SDS-PAGE loading buffer (final concentration 62.5 mM Tris, pH 6.8, 3% β–mercaptoethanol, 8% SDS, 15% glycerol) at 95°C for 5 min. Afterward, samples were electrophoresed and transferred to a polyvinylidene difluoride membrane (Millipore); the membrane was blocked for 30 min with blocking buffer (5% nonfat dry milk, 50 mM Tris-HCl, pH 7.5, 0.05% Tween-20). After extensive washing with TBS containing 0.1% Tween-20, the immunoblots were incubated with primary antibodies for 2 h. Antibody binding was detected using an IRDye 800–conjugated goat anti-mouse IgG (LI-COR Bioscience) or IRDye 680–conjugated goat anti-rabbit IgG (LI-COR Bioscience) and visualized with an ODYSSEY infrared imaging system (LI-COR Bioscience). For quantification of kininogen immunoblots, the density of immunoblots was calculated using Quantity one software (Bio-Rad); the density of the blots in all film were background-subtracted and reported as adjusted volume ($INT \times mm^2$).

BODIPY FL labeling of LPS
To prepare a conjugate of LPS with BODIPY FL, LPS was suspended at 2 mg/ml in 0.25 ml PBS, sonicated, and mixed with 25 µl 50 mM BODIPY FL hydrazide in dimethyl sulfoxide. After incubation at 37°C for 40 min, the mixture was sonicated again, 0.2 ml 0.2 M $NaHCO_3$, pH 8.7, and another 25 µl BODIPY FL hydrazide were added, and the incubation was continued for 1 h. The sample was microcentrifuged, and the supernatant was dialyzed. The labeling of BODIPY FL dye was determined by measurement of optical density at 503 nm.

Measurement of fluorescence of BODIPY FL–LPS
To measure the time-dependent changes in fluorescence levels that occur upon disaggregation of BODIPY FL–LPS, the fluorescence was measured over 600 s in 20-s intervals after the quick addition of HK, HKa, LC, or HC to 100 µl BODIPY FL-LPS in PBS. LBP mixed with sCD14 was used as a positive control. Because 2% SDS completely solubilizes LPS, the increase in BODIPY FL fluorescence level under these conditions represents the fully disaggregated state of LPS (100% disaggregation). The relative fluorescence intensities (%) were calculated based on the fluorescence measured in the presence of 2% SDS.

Binding of FITC–LPS to HK
Ninety-six-well Fluotrac 600 high-binding plates were coated with 10 µg/ml HKa in 50 mM carbonate/bicarbonate buffer or BSA at 4°C overnight. After washing with PBS, the wells were blocked with 2% BSA in PBS at room temperature for 1 h. After washing, the wells were incubated with 100 µg/ml FITC-LPS in the presence or absence of 50 µM $ZnCl_2$ at 37°C. The wells were then washed three times, followed by measurement of fluorescence ($\lambda ex = 495$ nm, $\lambda em = 515$ nm).

Chromatography
HK, in the presence or absence of LPS, was analyzed using a Superdex 200 10/300 GL (1 × 30 cm) size–exclusion column connected to an FPLC instrument (AKTA; GE Healthcare). LPS (250 µg/ml) was incubated with 50 µg/ml HK at 37°C for 60 min in PBS in a final volume of 200 µl. Samples were then loaded onto the column that was equilibrated with PBS, which was also used as the elution buffer at a flow rate of 0.6 ml/min. The absorbance was monitored at 210 and 280 nm. The fractions corresponding to the HK/LPS peak were collected and pooled. The concentration of HK was determined by the bicinchoninic acid assay using BSA as a standard. The LAL assay was used to determine LPS concentrations.

Generation of C11C1 mAb and anti-DHG15 antibody
The hybridoma producing mAb C11C1 was generated as previously described (Song et al., 2004; Khan et al., 2010) and purified by GenScript. An anti-DHG15 antibody was produced by GenScript, using a peptide (DHGHKHKHG HGHGKHC conjugated with KLH) HPLC purified to >96% purity as immunogen.

Data analysis
Data are expressed as mean ± SEM from at least three independent experiments unless otherwise indicated. Data were analyzed using GraphPad Prism 5. For parametric comparisons, a one-way ANOVA followed by Tukey's test for multiple groups and a two-tailed Student's t test for two groups were used. As previously described, Kaplan-Meier survival curves were generated, and comparisons of median survival were performed using log-rank and Gehan-Breslow-Wilcoxon

tests (Chalastanis et al., 2010). P-values of <0.05 were considered to indicate statistical significance.

Online supplemental material

Fig. S1 provides a description of the generation and characterization of $Kng1^{-/-}$ mice. Fig. S2 shows that HK interaction with LPS is not dependent of Zn^{2+}. Fig. S3 indicates disaggregation of *E. coli* 055:B5 LPS and *S. minnesota* LPS by HKa. Fig. S4 shows that LC enhances LPS-stimulated TNF production. Fig. S5 shows that reconstitution of $Kng1^{-/-}$ mice with a mutant HK lacking the DHG15 region fails to recover plasma LPS levels.

REFERENCES

Baik, J.E., S.W. Hong, S. Choi, J.H. Jeon, O.J. Park, K. Cho, D.G. Seo, K.Y. Kum, C.H. Yun, and S.H. Han. 2013. Alpha-amylase is a human salivary protein with affinity to lipopolysaccharide of *Aggregatibacter actinomycetemcomitans*. *Mol. Oral Microbiol.* 28:142–153. http://dx.doi.org/10.1111/omi.12011

Cagliani, R., D. Forni, S. Riva, U. Pozzoli, M. Colleoni, N. Bresolin, M. Clerici, and M. Sironi. 2013. Evolutionary analysis of the contact system indicates that kininogen evolved adaptively in mammals and in human populations. *Mol. Biol. Evol.* 30:1397–1408. http://dx.doi.org/10.1093/molbev/mst054

Chalastanis, A., V. Penard-Lacronique, M. Svrcek, V. Defaweux, N. Antoine, O. Buhard, S. Dumont, B. Fabiani, I. Renault, E. Tubacher, et al. 2010. Azathioprine-induced carcinogenesis in mice according to Msh2 genotype. *J. Natl. Cancer Inst.* 102:1731–1740. http://dx.doi.org/10.1093/jnci/djq389

Champion, K., L. Chiu, J. Ferbas, and M. Pepe. 2013. Endotoxin neutralization as a biomonitor for inflammatory bowel disease. *PLoS One.* 8:e67736. http://dx.doi.org/10.1371/journal.pone.0067736

Cohen, J., J.-L. Vincent, N.K.J. Adhikari, F.R. Machado, D.C. Angus, T. Calandra, K. Jaton, S. Giulieri, J. Delaloye, S. Opal, et al. 2015. Sepsis: a roadmap for future research. *Lancet Infect. Dis.* 15:581–614. http://dx.doi.org/10.1016/S1473-3099(15)70112-X

Colman, R.W. 1994. The contact system and sepsis. *Prog. Clin. Biol. Res.* 388:195–214.

Colman, R.W., and A.H. Schmaier. 1997. Contact system: a vascular biology modulator with anticoagulant, profibrinolytic, antiadhesive, and proinflammatory attributes. *Blood.* 90:3819–3843.

Dai, J., A. Agelan, A. Yang, V. Zuluaga, D. Sexton, R.W. Colman, and Y. Wu. 2012. Role of plasma kallikrein-kinin system activation in synovial

recruitment of endothelial progenitor cells in experimental arthritis. *Arthritis Rheum.* 64:3574–3582. http://dx.doi.org/10.1002/art.34607

Das, S., K.A. Owen, K.T. Ly, D. Park, S.G. Black, J.M. Wilson, C.D. Sifri, K.S. Ravichandran, P.B. Ernst, and J.E. Casanova. 2011. Brain angiogenesis inhibitor 1 (BAI1) is a pattern recognition receptor that mediates macrophage binding and engulfment of Gram-negative bacteria. *Proc. Natl. Acad. Sci. USA.* 108:2136–2141. http://dx.doi.org/10.1073/pnas.1014775108

Davies, B., and J. Cohen. 2011. Endotoxin removal devices for the treatment of sepsis and septic shock. *Lancet Infect. Dis.* 11:65–71. http://dx.doi.org/10.1016/S1473-3099(10)70220-6

DeLa Cadena, R.A., A.F. Suffredini, J.D. Page, R.A. Pixley, N. Kaufman, J.E. Parrillo, and R.W. Colman. 1993. Activation of the kallikrein-kinin system after endotoxin administration to normal human volunteers. *Blood.* 81:3313–3317.

Doolittle, R.F. 2011. Coagulation in vertebrates with a focus on evolution and inflammation. *J. Innate Immun.* 3:9–16. http://dx.doi.org/10.1159/000321005

Fang, C., E. Stavrou, A.A. Schmaier, N. Grobe, M. Morris, A. Chen, M.T. Nieman, G.N. Adams, G. LaRusch, Y. Zhou, et al. 2013. Angiotensin 1-7 and Mas decrease thrombosis in Bdkrb2-/- mice by increasing NO and prostacyclin to reduce platelet spreading and glycoprotein VI activation. *Blood.* 121:3023–3032. http://dx.doi.org/10.1182/blood-2012-09-459156

Gallimore, M.J., A.O. Aasen, K.H.N. Lyngaas, M. Larsbraaten, and E. Amundsen. 1978. Falls in plasma levels of prekallikrein, high molecular weight kininogen, and kallikrein inhibitors during lethal endotoxin shock in dogs. *Thromb. Res.* 12:307–318. http://dx.doi.org/10.1016/0049-3848(78)90301-8

Gotts, J.E., and M.A. Matthay. 2016. Sepsis: pathophysiology and clinical management. *BMJ.* 353:i1585. http://dx.doi.org/10.1136/bmj.i1585

Grailer, J.J., B.A. Canning, M. Kalbitz, M.D. Haggadone, R.M. Dhond, A.V. Andjelkovic, F.S. Zetoune, and P.A. Ward. 2014. Critical role for the NLRP3 inflammasome during acute lung injury. *J. Immunol.* 192:5974–5983. http://dx.doi.org/10.4049/jimmunol.1400368

Hack, C.E., and R.W. Colman. 1999. The role of the contact system in the pathogenesis of septic shock. *Sepsis.* 3:111–118. http://dx.doi.org/10.1023/A:1009895315442

Håkansson, H.F., A. Smailagic, C. Brunmark, A. Miller-Larsson, and H. Lal. 2012. Altered lung function relates to inflammation in an acute LPS mouse model. *Pulm. Pharmacol. Ther.* 25:399–406. http://dx.doi.org/10.1016/j.pupt.2012.08.001

Harm, S., D. Falkenhagen, and J. Hartmann. 2014. Endotoxin adsorbents in extracorporeal blood purification: do they fulfill expectations? *Int. J. Artif. Organs.* 37:222–232. http://dx.doi.org/10.5301/ijao.5000304

Haziot, A., E. Ferrero, F. Köntgen, N. Hijiya, S. Yamamoto, J. Silver, C.L. Stewart, and S.M. Goyert. 1996. Resistance to endotoxin shock and reduced dissemination of gram-negative bacteria in CD14-deficient mice. *Immunity.* 4:407–414. http://dx.doi.org/10.1016/S1074-7613(00)80254-X

Heinzelmann, M., and H. Bosshart. 2005. Heparin binds to lipopolysaccharide (LPS)-binding protein, facilitates the transfer of LPS to CD14, and enhances LPS-induced activation of peripheral blood monocytes. *J. Immunol.* 174:2280–2287. http://dx.doi.org/10.4049/jimmunol.174.4.2280

Herwald, H., M. Mörgelin, B. Dahlbäck, and L. Björck. 2003. Interactions between surface proteins of Streptococcus pyogenes and coagulation factors modulate clotting of human plasma. *J. Thromb. Haemost.* 1:284–291. http://dx.doi.org/10.1046/j.1538-7836.2003.00105.x

Hoshino, K., O. Takeuchi, T. Kawai, H. Sanjo, T. Ogawa, Y. Takeda, K. Takeda, and S. Akira. 1999. Cutting edge: Toll-like receptor 4 (TLR4)-deficient mice are hyporesponsive to lipopolysaccharide: evidence for TLR4 as the Lps gene product. *J. Immunol.* 162:3749–3752.

Huebener, P., J.-P. Pradere, C. Hernandez, G.-Y. Gwak, J.M. Caviglia, X. Mu, J.D. Loike, R.E. Jenkins, D.J. Antoine, and R.F. Schwabe. 2015. The HMGB1/RAGE axis triggers neutrophil-mediated injury amplification following necrosis. *J. Clin. Invest.* 125:539–550. http://dx.doi.org/10.1172/JCI76887

Hyakushima, N., H. Mitsuzawa, C. Nishitani, H. Sano, K. Kuronuma, M. Konishi, T. Himi, K. Miyake, and Y. Kuroki. 2004. Interaction of soluble form of recombinant extracellular TLR4 domain with MD-2 enables lipopolysaccharide binding and attenuates TLR4–mediated signaling. *J. Immunol.* 173:6949–6954. http://dx.doi.org/10.4049/jimmunol.173.11.6949

Jack, R.S., X. Fan, M. Bernheiden, G. Rune, M. Ehlers, A. Weber, G. Kirsch, R. Mentel, B. Fürll, M. Freudenberg, et al. 1997. Lipopolysaccharide-binding protein is required to combat a murine gram-negative bacterial infection. *Nature.* 389:742–745. http://dx.doi.org/10.1038/39622

Jansen, P.M., R.A. Pixley, M. Brouwer, I.W. de Jong, A.C. Chang, C.E. Hack, F.B. Taylor Jr., and R.W. Colman. 1996. Inhibition of factor XII in septic baboons attenuates the activation of complement and fibrinolytic systems and reduces the release of interleukin-6 and neutrophil elastase. *Blood.* 87:2337–2344.

Khan, M.M., H.N. Bradford, I. Isordia-Salas, Y. Liu, Y. Wu, R.G. Espinola, B. Ghebrehiwet, and R.W. Colman. 2006. High-molecular-weight kininogen fragments stimulate the secretion of cytokines and chemokines through uPAR, Mac-1, and gC1qR in monocytes. *Arterioscler. Thromb. Vasc. Biol.* 26:2260–2266. http://dx.doi.org/10.1161/01.ATV.0000240290.70852.c0

Khan, S.T., R.A. Pixley, Y. Liu, N. Bakdash, B. Gordon, A. Agelan, Y. Huang, M.P. Achary, and R.W. Colman. 2010. Inhibition of metastasis of syngeneic murine melanoma in vivo and vasculogenesis in vitro by monoclonal antibody C11C1 targeted to domain 5 of high molecular weight kininogen. *Cancer Immunol. Immunother.* 59:1885–1893. http://dx.doi.org/10.1007/s00262-010-0915-0

Kimball, H.R., M.L. Melmon, and S.M. Wolff. 1972. Endotoxin-induced kinin production in man. *Proc. Soc. Exp. Biol. Med.* 139:1078–1082. http://dx.doi.org/10.3181/00379727-139-36302

Kos, J., M. Dolinar, and V. Turk. 1992. Isolation and characterisation of chicken L- and H-kininogens and their interaction with chicken cysteine proteinases and papain. *Agents Actions Suppl.* 38:331–339.

Langhauser, F., E. Göb, P. Kraft, C. Geis, J. Schmitt, M. Brede, K. Göbel, X. Helluy, M. Pham, M. Bendszus, et al. 2012. Kininogen deficiency protects from ischemic neurodegeneration in mice by reducing thrombosis, blood-brain barrier damage, and inflammation. *Blood.* 120:4082–4092. http://dx.doi.org/10.1182/blood-2012-06-440057

Lei, M.G., and D.C. Morrison. 1988. Specific endotoxic lipopolysaccharide-binding proteins on murine splenocytes. II. Membrane localization and binding characteristics. *J. Immunol.* 141:1006–1011.

Le Roy, D., F. Di Padova, R. Tees, S. Lengacher, R. Landmann, M.P. Glauser, T. Calandra, and D. Heumann. 1999. Monoclonal antibodies to murine lipopolysaccharide (LPS)-binding protein (LBP) protect mice from lethal endotoxemia by blocking either the binding of LPS to LBP or the presentation of LPS/LBP complexes to CD14. *J. Immunol.* 162:7454–7460.

Li, L., Y. Ling, M. Huang, T. Yin, S.-M. Gou, N.-Y. Zhan, J.-X. Xiong, H.-S. Wu, Z.-Y. Yang, and C.-Y. Wang. 2015. Heparin inhibits the inflammatory response induced by LPS and HMGB1 by blocking the binding of HMGB1 to the surface of macrophages. *Cytokine.* 72:36–42. http://dx.doi.org/10.1016/j.cyto.2014.12.010

Lin, B., H. Meng, H. Bing, D. Zhangsun, and S. Luo. 2014. Efficient expression of acetylcholine-binding protein from Aplysia californica in Bac-to-Bac system. *BioMed Res. Int.* 2014:691480. http://dx.doi.org/10.1155/2014/691480

Martínez-Brotóns, F., J.R. Oncins, J. Mestres, V. Amargós, and C. Reynaldo. 1987. Plasma kallikrein-kinin system in patients with uncomplicated sepsis and septic shock—comparison with cardiogenic shock. *Thromb. Haemost.* 58:709–713.

Mason, J.W., U. Kleeberg, P. Dolan, and R.W. Colman. 1970. Plasma kallikrein and Hageman factor in Gram-negative bacteremia. *Ann. Intern. Med.* 73:545–551. http://dx.doi.org/10.7326/0003-4819-73-4-545

Merkulov, S., W.-M. Zhang, A.A. Komar, A.H. Schmaier, E. Barnes, Y. Zhou, X. Lu, T. Iwaki, F.J. Castellino, G. Luo, and K.R. McCrae. 2008. Deletion of murine kininogen gene 1 (mKng1) causes loss of plasma kininogen and delays thrombosis. *Blood.* 111:1274–1281. http://dx.doi.org/10.1182/blood-2007-06-092338

Moon, A., S. Gil, S.E. Gill, P. Chen, and G. Matute-Bello. 2012. Doxycycline impairs neutrophil migration to the airspaces of the lung in mice exposed to intratracheal lipopolysaccharide. *J. Inflamm. (Lond.).* 9:31. http://dx.doi.org/10.1186/1476-9255-9-31

Morrison, D.C., and C.G. Cochrane. 1974. Direct evidence for Hageman factor (factor XII) activation by bacterial lipopolysaccharides (endotoxins). *J. Exp. Med.* 140:797–811. http://dx.doi.org/10.1084/jem.140.3.797

Nagai, Y., S. Akashi, M. Nagafuku, M. Ogata, Y. Iwakura, S. Akira, T. Kitamura, A. Kosugi, M. Kimoto, and K. Miyake. 2002. Essential role of MD-2 in LPS responsiveness and TLR4 distribution. *Nat. Immunol.* 3:667–672.

Oehmcke, S., M. Mörgelin, and H. Herwald. 2009. Activation of the human contact system on neutrophil extracellular traps. *J. Innate Immun.* 1:225–230. http://dx.doi.org/10.1159/000203700

Pais de Barros, J.-P., T. Gautier, W. Sali, C. Adrie, H. Choubley, E. Charron, C. Lalande, N. Le Guern, V. Deckert, M. Monchi, et al. 2015. Quantitative lipopolysaccharide analysis using HPLC/MS/MS and its combination with the limulus amebocyte lysate assay. *J. Lipid Res.* 56:1363–1369. http://dx.doi.org/10.1194/jlr.D059725

Paloma, M.J., J.A. Páramo, and E. Rocha. 1992. Effect of DDAVP on endotoxin-induced intravascular coagulation in rabbits. *Thromb. Haemost.* 68:306–309.

Park, B.S., and J.-O. Lee. 2013. Recognition of lipopolysaccharide pattern by TLR4 complexes. *Exp. Mol. Med.* 45:e66. http://dx.doi.org/10.1038/emm.2013.97

Pixley, R.A., R.A. DeLa Cadena, J.D. Page, N. Kaufman, E.G. Wyshock, R.W. Colman, A. Chang, and F.B. Taylor Jr. 1992. Activation of the contact system in lethal hypotensive bacteremia in a baboon model. *Am. J. Pathol.* 140:897–906.

Pixley, R.A., Y. Lin, I. Isordia-Salas, and R.W. Colman. 2003. Fine mapping of the sequences in domain 5 of high molecular weight kininogen (HK) interacting with heparin and zinc. *J. Thromb. Haemost.* 1:1791–1798. http://dx.doi.org/10.1046/j.1538-7836.2003.00291.x

Reddigari, S., and A.P. Kaplan. 1989. Quantification of human high molecular weight kininogen by immunoblotting with a monoclonal anti-light chain antibody. *J. Immunol. Methods.* 119:19–25. http://dx.doi.org/10.1016/0022-1759(89)90376-1

Roeise, O., B.N. Bouma, J.O. Stadaas, and A.O. Aasen. 1988. Dose dependence of endotoxin-induced activation of the plasma contact system: an in vitro study. *Circ. Shock.* 26:419–430.

Ronco, C. 2014. Endotoxin removal: history of a mission. *Blood Purif.* 37(s1, Suppl 1):5–8. http://dx.doi.org/10.1159/000356831

Song, J.S., I.M. Sainz, S.C. Cosenza, I. Isordia-Salas, A. Bior, H.N. Bradford, Y.-L. Guo, R.A. Pixley, E.P. Reddy, and R.W. Colman. 2004. Inhibition of tumor angiogenesis in vivo by a monoclonal antibody targeted to domain 5 of high molecular weight kininogen. *Blood.* 104:2065–2072. http://dx.doi.org/10.1182/blood-2004-02-0449

Wang, Z.-Q., W.-M. Xing, H.-H. Fan, K.-S. Wang, H.-K. Zhang, Q.-W. Wang, J. Qi, H.-M. Yang, J. Yang, Y.-N. Ren, et al. 2009. The novel lipopolysaccharide-binding protein CRISPLD2 is a critical serum protein to regulate endotoxin function. *J. Immunol.* 183:6646–6656. http://dx.doi.org/10.4049/jimmunol.0802348

Wu, Y. 2015. Contact pathway of coagulation and inflammation. *Thromb. J.* 13:17. http://dx.doi.org/10.1186/s12959-015-0048-y

Wurfel, M.M., B.G. Monks, R.R. Ingalls, R.L. Dedrick, R. Delude, D. Zhou, N. Lamping, R.R. Schumann, R. Thieringer, M.J. Fenton, et al. 1997. Targeted deletion of the lipopolysaccharide (LPS)-binding protein gene leads to profound suppression of LPS responses ex vivo, whereas in vivo responses remain intact. *J. Exp. Med.* 186:2051–2056. http://dx.doi.org/10.1084/jem.186.12.2051

Xie, Z., J. Dai, A. Yang, and Y. Wu. 2014. A role for bradykinin in the development of anti-collagen antibody-induced arthritis. *Rheumatology (Oxford).* 53:1301–1306. http://dx.doi.org/10.1093/rheumatology/keu015

Yanai, H., T. Ban, Z. Wang, M.K. Choi, T. Kawamura, H. Negishi, M. Nakasato, Y. Lu, S. Hangai, R. Koshiba, et al. 2009. HMGB proteins function as universal sentinels for nucleic-acid-mediated innate immune responses. *Nature.* 462:99–103. http://dx.doi.org/10.1038/nature08512

Yang, A., J. Dai, Z. Xie, R.W. Colman, Q. Wu, R.B. Birge, and Y. Wu. 2014. High molecular weight kininogen binds phosphatidylserine and opsonizes urokinase plasminogen activator receptor-mediated efferocytosis. *J. Immunol.* 192:4398–4408. http://dx.doi.org/10.4049/jimmunol.1302590

Youn, J.H., Y.J. Oh, E.S. Kim, J.E. Choi, and J.-S. Shin. 2008. High mobility group box 1 protein binding to lipopolysaccharide facilitates transfer of lipopolysaccharide to CD14 and enhances lipopolysaccharide-mediated TNF-α production in human monocytes. *J. Immunol.* 180:5067–5074. http://dx.doi.org/10.4049/jimmunol.180.7.5067

Zhang, H., A.T. Kho, Q. Wu, A.J. Halayko, K. Limbert Rempel, R.P. Chase, N.B. Sweezey, S.T. Weiss, and F. Kaplan. 2016. CRISPLD2 (LGL1) inhibits proinflammatory mediators in human fetal, adult, and COPD lung fibroblasts and epithelial cells. *Physiol. Rep.* 4:e12942. http://dx.doi.org/10.14814/phy2.12942

Zhou, J., Y. Wu, L. Wang, L. Rauova, V.M. Hayes, M. Poncz, and D.W. Essex. 2015. The C-terminal CGHC motif of protein disulfide isomerase supports thrombosis. *J. Clin. Invest.* 125:4391–4406. http://dx.doi.org/10.1172/JCI80319

Zhou, L., J. Li-Ling, H. Huang, F. Ma, and Q. Li. 2008. Phylogenetic analysis of vertebrate kininogen genes. *Genomics.* 91:129–141. http://dx.doi.org/10.1016/j.ygeno.2007.10.007